Guided waves propagation in arbitrarily stacked composite laminates: Between-layers incompatibility issue resolution using hybrid matrix strategy

Shuanglin Guo [a,*], Marc Rébillat [b], Yuan Liu [a], Qiufeng Li [a], Chao Lu [a], Nazih Mechbal [b]

[a] Key Laboratory of Nondestructive Testing, Ministry of Education, Nanchang Hangkong University, Nanchang, 330063, China
[b] PIMM, Arts et Metiers Institute of Technology, CNRS, Cnam, HESAM University, 151 boulevard de l'Hopital, Paris, 75013, France

ARTICLE INFO

Keywords:
Guided waves
Metallic-composite laminate
Stiffness matrix method
Incompatibility issue
Hybrid matrix strategy

ABSTRACT

Lamb waves (LWs) are widely used to achieve structural health monitoring of aeronautic composite structures. Composite materials are however anisotropic and LWs propagation characteristics depend on their propagation direction. Within one composite ply, when this direction coincides with the principal axis of the ply, they are not coupled with shear waves (SHWs) but become coupled with SHWs for any other direction. As composite materials are built up with layers at various orientations LWs and SHWs are coupled for some layers and uncoupled for some others when studying an arbitrary propagation direction. Transfer Matrix Method (TMM), Global Matrix Method (GMM), and Stiffness Matrix Method (SMM) are all methods allowing to predict guided waves (LWs and SHWs) behavior in composite materials. However those methods suffer from an incompatibility issue preventing them to manage cases when SHWs and LWs are coupled for some plies but uncoupled for some other plies. This issue is particularly frequent when dealing with metallic-composite plates or with composite plates made up with isotropic, orthotropic, and triclinic materials. In order to solve this incompatibility issue, a hybrid matrix strategy (HMS) is proposed here on the basis of SMM. The core idea of the HMS is to re-couple LWs and SHWs into hybrid guided waves when they are uncoupled in order to make them compatible with the general coupled waves cases. The numerical stability of HMS is proved theoretically and its effectiveness is validated through numerical investigations and using experimental data from the literature. The SMM-HMS framework can thus be considered as a state of the art benchmark approach for evaluating the performance of numerical methods dedicated to the computation of guided waves dispersion curves and can be confidently applied to any arbitrary composite material used in aeronautic and aerospace industries.

1. Introduction

Carbon fiber reinforced plastics (CFRP) composite materials are widely used in aeronautic and aerospace industries thanks to their high strength-to-weight ratio [1]. However, composite materials generally undergo complex damage mechanisms during the manufacturing or in-service process, for instance, delamination, matrix cracking, fiber breakage, etc. [2]. To secure the integrity and durability of composite structures, guided wave-based structural health monitoring (SHM) techniques grow into reliable solutions in recent years to prevent catastrophic failure of aerospace composite structures [3,4]. Akin to the well-known Lamb waves [5,6], guided waves hold dispersion and multi-modal properties, which describe the wave velocity dependence on frequency and mode order [7]. Understanding the dispersion behavior of guided waves is the premise for performing a guided wave-based SHM system as it determines the choice of excitation frequency and desired wave mode [8]. Thus, a multitude of works in the literature is devoted to building analytical or numerical models for obtaining the dispersion curves of multi-layered composite plates [9,10].

The analytical models mainly refer to the matrix-based methods, containing the transfer matrix method (TMM) [11,12], global matrix method (GMM) [13,14], and stiffness matrix method (SMM) [15,16]. The linear 3D elasticity theory is the theoretical basis of the matrix-based methods [17], and hence this class of method becomes the benchmark for evaluating the performance of other methods [9,10,18,19]. Matrix-based methods usually start with the analysis of partial waves in a single lamina by deriving the Christoffel equation. This procedure is usually denominated as the partial wave superposition approach (PWSA) in the literature [20–22]. For the multi-layered plate system, PWSA is extended to the three aforementioned matrix-based methods according to the different ways of applying the interface continuity condition and the traction-free boundary condition [1,12].

* Corresponding author.
E-mail address: guo.shuanglin@nchu.edu.cn (S. Guo).

[1] fd means the product of frequency f and plate's thickness d.

In contrast with TMM usually encountering the *large fd problem*[1] [14,23], the main advantage of GMM rests on its numerical stability even at large fd range but at the cost of increasing computational burden [14,17]. Ramasawmy et al. employed GMM to develop the MATLAB toolbox *ElasticMatrix* for computing the dispersion curves of transversely isotropic material along its principal direction [24]. Lowe developed the commercial software *Disperse* based on GMM that became the pioneering computing program in the past two decades [25]. It has been proved that SMM is unconditionally stable [16], thus it is becoming the prevalent way of computing dispersion curves of composite laminates in recent years [26,27]. Huber et al. adopted SMM to create the stand-alone freeware *Dispersion Calculator* [28]. Notwithstanding the unconditionally stable at large fd range, SMM becomes unstable if the thickness of one layer of the laminate is close to zero. Tan proposed the hybrid compliance-stiffness matrix method (HCSMM) to resolve this issue [29–32].

There are multifarious numerical methods in the literature. The mainstream one is the semi-analytical finite element method (SAFE), benefiting from the flexible discretization in the cross-section of waveguide, SAFE has natural advantage for modeling wave propagation in waveguides of arbitrary cross-section [33]. Bocchini et al. developed the freeware *GUIGUW* [34] based on SAFE to compute dispersion curves of various waveguides containing composite laminate, cylinder, circular tube, square tube and railroad tracks, etc. To take full advantage of the commercial FEM software such as ANSYS, the wave finite element method (WFEM) was developed by Mace and Manconi [35] and Sorohan et al. [36]. Given that the wavelength changes with frequency, the elements adopted in WFEM in the propagation direction should be re-meshed for different frequencies to retain the consistent accuracy [36], thus it is not as flexible as SAFE. The spectral collocation method (SCM) based on Chebyshev polynomials [18,37] has also been employed to model guided wave propagation, that allocates spectral points in the thickness direction to discretize each layer of a laminate, instead of elements in SAFE and WFEM. This method shows asset in computing the full 3D dispersion curves of anisotropic viscoelastic media [38] and is being developed for leaky wave characterization [39, 40].

The remaining numerical methods available from the literature are the higher order plate theory method (HOPT) [41–43], Legendre polynomial method (LPM) [44–46], Ritz-Rayleigh method [47,48], Green's function [49], and Green's matrix method [50]. These methods keep the approximation property that at larger frequency range or for the higher order modes, they generally produce a poor accuracy of solutions. This phenomenon has been validated by the open source software *The Dispersion Box* developed by Orta et al. [10] who made a comparative study for GMM, SMM, HCSMM, SAFE, LPM and HOPT.

In composite plate waveguides, there is a convention in the literature that two cases are separately addressed: one is for the decoupled Lamb and shear-horizontal (SH) waves for the propagation direction along the principal axis of composite material [21]; another is for the coupled ones when the propagation is oriented at the off-principal axis direction [51]. In addition to the two previously mentioned stereotypes, for complex aerospace composite laminates having arbitrary stacking angles, there is one special case that the wave propagation direction of interest may coincide with the principal direction of some laminae but could orient at the off-principal direction of other laminae due to the varying stacking angles of layups [52]. For this particular case, there exists an interlaminar mismatch issue in terms of fiber direction, and hence, a mismatch issue of wave types among laminae, which will further lead to numerical instability when implementing dispersion curves generating algorithms [17,53]. This kind of issues become more salient in the fiber-metal laminates given that there is a significant difference between the Young's modulus of the CFRP and metallic layers [54].

As a consequence, finding a way allowing to unite the various wave types in different laminae in order to overcome the mismatch issue becomes an essential concern, which has not been comprehensively studied in the literature [21,53]. In this paper, the hybrid matrix strategy (HMS) associated with SMM is proposed to resolve this issue. HMS means that the stiffness matrices of Lamb and SH waves will be recast into a hybrid form to *recouple* the pure Lamb and SH waves. HMS is straightforward, intuitional and numerically stable. It should be clarified that HMS is original and different from Tan's HCSMM introduced previously, which was devoted to dealing with the instability issue of SMM when the thickness of one layer of laminate is close to zero [30].

This paper is structured as follows. In Section 2, the guided waves propagation in a single lamina with various anisotropic materials is derived that defines the PWSA. In Section 3, the stiffness matrix method is investigated to derive the dispersion equation of guided waves propagation in arbitrarily stacked composite laminates. The incompatibility issue is highlighted in Section 4 and HMS is originally proposed to cope with this issue. Section 5 provides various numerical examples to validate this strategy. Discussion and conclusion are presented in sections 6 and 7, respectively.

2. Waves propagation in a lamina

2.1. Basic equations of 3D elasticity

Waves propagation in solid materials, as a typical elasticity problem, is physically characterized by the stress tensor σ_{ij}, strain tensor ε_{ij} and displacement tensor u_i. These quantities must satisfy the basic equations of 3D elasticity, i.e. the general Hooke's law of Eq. (1), the geometrical equations of Eq. (2), and the elastodynamic equations of Eq. (3).

$$\sigma_{ij} = c_{ijkl}\varepsilon_{kl} \quad (i,j,k,l = 1,2,3) \tag{1}$$

$$\varepsilon_{kl} = \frac{1}{2}(u_{k,l} + u_{l,k}) \quad (k,l = 1,2,3) \tag{2}$$

$$c_{ijkl}u_{l,kj} = \rho\ddot{u}_i \quad (i = 1,2,3) \tag{3}$$

where, c_{ijkl} is the fourth order elastic tensor having symmetric property, ρ is the mass density. Note that in Eqs. (1) and (3) the Einstein summation convention is implied for the repeated indices.

Eq. (1) of the tensor form can be transformed to the Eq. (4) of the matrix form through the Voigt notation with the one-to-one correspondence ij or $kl = 11, 22, 33, 23(32), 13(31), 12(21) \leftrightarrow p$ or $q = 1,2,3,4,5,6$.

$$\begin{bmatrix}\sigma_{11}\\ \sigma_{22}\\ \sigma_{33}\\ \sigma_{23}\\ \sigma_{13}\\ \sigma_{12}\end{bmatrix} = \begin{bmatrix} C_{11} & C_{12} & C_{13} & C_{14} & C_{15} & C_{16} \\ & C_{22} & C_{23} & C_{24} & C_{25} & C_{26} \\ & & C_{33} & C_{34} & C_{35} & C_{36} \\ & & & C_{44} & C_{45} & C_{46} \\ & \text{sym} & & & C_{55} & C_{56} \\ & & & & & C_{66} \end{bmatrix} \begin{bmatrix}\varepsilon_{11}\\ \varepsilon_{22}\\ \varepsilon_{33}\\ 2\varepsilon_{23}\\ 2\varepsilon_{13}\\ 2\varepsilon_{12}\end{bmatrix} \tag{4}$$

where, the matrix in Eq. (4) is the elastic matrix of the material which is symmetric and denoted by $\mathbf{C} \in \mathbb{C}^{6\times6}$.

In the elastic matrix $\mathbf{C}$ of Eq. (4), there are 21 prescribed independent non-zero elements. In material science, according to the behavior of crystal symmetry axes, materials are physically classified into six formats, specifically, triclinic ($\mathbf{C}_\mathrm{T}$), monoclinic ($\mathbf{C}_\mathrm{M}$), orthotropic ($\mathbf{C}_\mathrm{O}$), transversely isotropic ($\mathbf{C}_\mathrm{TI}$), cubic ($\mathbf{C}_\mathrm{C}$) and isotropic ($\mathbf{C}_\mathrm{I}$) materials [52, 55]. Mathematically, this classification is equivalent to count the different number of independent non-zero elements in the elastic matrix $\mathbf{C}$, in other words, depending on the format of matrix $\mathbf{C}$ summarized in the second column of Fig. 1.

In this paper, we define a uniform set notation to represent the six formats of elastic matrices, i.e. $\mathcal{C}_\mathcal{T}$, $\mathcal{C}_\mathcal{M}$, $\mathcal{C}_\mathcal{O}$, $\mathcal{C}_{\mathcal{TI}}$, $\mathcal{C}_\mathcal{C}$, $\mathcal{C}_\mathcal{I}$. We further stipulate $\mathcal{C}_\mathcal{M} \subseteq \mathcal{C}_\mathcal{T}$ and $\mathcal{C}_{\mathcal{TI}}, \mathcal{C}_\mathcal{C}, \mathcal{C}_\mathcal{I} \subseteq \mathcal{C}_\mathcal{O}$ as stated in the fourth column of Fig. 1, based on the fact that $\mathcal{C}_\mathcal{M}$ has the same property as $\mathcal{C}_\mathcal{T}$, and $\mathcal{C}_{\mathcal{TI}}, \mathcal{C}_\mathcal{C}, \mathcal{C}_\mathcal{I}$ have the same property as $\mathcal{C}_\mathcal{O}$ in terms of the coupling issue between Lamb and SH waves, which will be investigated in detail in the subsequent sections.

Material class	Format of elastic matrix $\mathbf{C}$ in the crystal axes coordinate system	Number of independent elements in $\mathbf{C}$	Property of elastic matrix $\mathbf{C}$	Property of the rotated elastic matrix $\mathbf{C}' = \mathrm{Rot}\{\mathbf{C}, \theta\}$
Triclinic material	$\mathbf{C}_\mathrm{T} = \begin{bmatrix} C_{11} & C_{12} & C_{13} & C_{14} & C_{15} & C_{16} \\ & C_{22} & C_{23} & C_{24} & C_{25} & C_{26} \\ & & C_{33} & C_{34} & C_{35} & C_{36} \\ & & & C_{44} & C_{45} & C_{46} \\ & \mathrm{sym} & & & C_{55} & C_{56} \\ & & & & & C_{66} \end{bmatrix}$	21	$\mathbf{C}_\mathrm{T} \in \mathcal{C}_\mathcal{T}$	$\mathbf{C}'_\mathrm{T} \in \mathcal{C}_\mathcal{T}$ for any θ
Monoclinic material	$\mathbf{C}_\mathrm{M} = \begin{bmatrix} C_{11} & C_{12} & C_{13} & 0 & 0 & C_{16} \\ & C_{22} & C_{23} & 0 & 0 & C_{26} \\ & & C_{33} & 0 & 0 & C_{36} \\ & & & C_{44} & C_{45} & 0 \\ & \mathrm{sym} & & & C_{55} & 0 \\ & & & & & C_{66} \end{bmatrix}$	13	$\mathbf{C}_\mathrm{M} \in \mathcal{C}_\mathcal{M}$ $(\mathcal{C}_\mathcal{M} \subseteq \mathcal{C}_\mathcal{T})$	$\mathbf{C}'_\mathrm{M} \in \mathcal{C}_\mathcal{M}$ for any θ
Orthotropic material	$\mathbf{C}_\mathrm{O} = \begin{bmatrix} C_{11} & C_{12} & C_{13} & 0 & 0 & 0 \\ & C_{22} & C_{23} & 0 & 0 & 0 \\ & & C_{33} & 0 & 0 & 0 \\ & & & C_{44} & 0 & 0 \\ & \mathrm{sym} & & & C_{55} & 0 \\ & & & & & C_{66} \end{bmatrix}$	9	$\mathbf{C}_\mathrm{O} \in \mathcal{C}_\mathcal{O}$	$\mathbf{C}'_\mathrm{O} \in \mathcal{C}_\mathcal{M}$ for $\theta \neq 90^\circ$ $\mathbf{C}'_\mathrm{O} \in \mathcal{C}_\mathcal{O}$ for $\theta = 90^\circ$
Transversely isotropic material	$\mathbf{C}_\mathrm{TI} = \begin{bmatrix} C_{11} & C_{12} & C_{12} & 0 & 0 & 0 \\ & C_{22} & C_{23} & 0 & 0 & 0 \\ & & C_{22} & 0 & 0 & 0 \\ & & & \frac{C_{22}-C_{23}}{2} & 0 & 0 \\ & \mathrm{sym} & & & C_{55} & 0 \\ & & & & & C_{55} \end{bmatrix}$	5	$\mathbf{C}_\mathrm{TI} \in \mathcal{C}_\mathcal{TJ}$ $(\mathcal{C}_\mathcal{TJ} \subseteq \mathcal{C}_\mathcal{O})$	$\mathbf{C}'_\mathrm{TI} \in \mathcal{C}_\mathcal{M}$ for $\theta \neq 90^\circ$ $\mathbf{C}'_\mathrm{TI} \in \mathcal{C}_\mathcal{O}$ for $\theta = 90^\circ$
Cubic material	$\mathbf{C}_\mathrm{C} = \begin{bmatrix} C_{11} & C_{12} & C_{12} & 0 & 0 & 0 \\ & C_{11} & C_{12} & 0 & 0 & 0 \\ & & C_{11} & 0 & 0 & 0 \\ & & & C_{44} & 0 & 0 \\ & \mathrm{sym} & & & C_{44} & 0 \\ & & & & & C_{44} \end{bmatrix}$	3	$\mathbf{C}_\mathrm{C} \in \mathcal{C}_\mathcal{C}$ $(\mathcal{C}_\mathcal{C} \subseteq \mathcal{C}_\mathcal{O})$	$\mathbf{C}'_\mathrm{C} \in \mathcal{C}_\mathcal{M}$ for $\theta \neq 45^\circ$ and 90° $\mathbf{C}'_\mathrm{C} \in \mathcal{C}_\mathcal{O}$ for $\theta = 45^\circ$ or 90°
Isotropic material	$\mathbf{C}_\mathrm{I} = \begin{bmatrix} C_{11} & C_{12} & C_{12} & 0 & 0 & 0 \\ & C_{11} & C_{12} & 0 & 0 & 0 \\ & & C_{11} & 0 & 0 & 0 \\ & & & \frac{C_{11}-C_{12}}{2} & 0 & 0 \\ & \mathrm{sym} & & & \frac{C_{11}-C_{12}}{2} & 0 \\ & & & & & \frac{C_{11}-C_{12}}{2} \end{bmatrix}$	2	$\mathbf{C}_\mathrm{I} \in \mathcal{C}_\mathcal{J}$ $(\mathcal{C}_\mathcal{J} \subseteq \mathcal{C}_\mathcal{O})$	$\mathbf{C}'_\mathrm{I} \in \mathcal{C}_\mathcal{J}$ for any θ

The red terms in various matrix $\mathbf{C}$ denote the independent non-zero elements.

Fig. 1. Elastic matrix formats of various material classes.

2.2. Elastic matrix rotation

It is conventional that the format of $\mathbf{C}$ in the second column of Fig. 1 is defined in the respective material's crystal axes system, for instance, the principal axis x_1 illustrated in Fig. 2(a). However, in a single lamina, guided waves can propagate at a general off-principal axis direction (x'_1 as illustrated in Fig. 2(a)). Thus, it is necessary to study the formats of elastic matrices of the six material classes along the off-principal axis direction θ. This can be achieved by using the matrix rotation formula [1] wrote in Eq. (5).

$$\mathbf{C}' = \mathbf{T}\mathbf{C}\mathbf{T}^\mathsf{T} \rightarrow \mathbf{C}' = \mathrm{Rot}\{\mathbf{C}, \theta\} \tag{5}$$

$$\mathbf{T} = \begin{bmatrix} c^2 & s^2 & 0 & 0 & 0 & 2cs \\ s^2 & c^2 & 0 & 0 & 0 & -2cs \\ 0 & 0 & 1 & 0 & 0 & 0 \\ 0 & 0 & 0 & c & -s & 0 \\ 0 & 0 & 0 & s & c & 0 \\ -cs & cs & 0 & 0 & 0 & c^2 - s^2 \end{bmatrix} \tag{6}$$

where, $\mathbf{T}$ is the rotation matrix; $c = \cos(\theta)$ and $s = \sin(\theta)$; θ is the rotation angle being positive for counterclockwise direction and negative for clockwise direction; the superscript T denotes the matrix transpose.

For ease comprehension, we define the notation $\mathbf{C}' = \mathrm{Rot}\{\mathbf{C}, \theta\}$ to represent the elastic matrix rotation formulized in Eq. (5). Thus, for the six material classes in Fig. 1, the property of the rotated elastic matrix is summarized in the last column of Fig. 1. The deriving process can be accessed from [22]. Here, we take the orthotropic material $\mathbf{C}_\mathrm{O}$ as the example to illustrate the property of the elastic matrix rotation. See the last column of Fig. 1 and focus on the row of orthotropic material.

- When $\theta \neq 90°$, the rotated matrix of the orthotropic material $\mathbf{C}'_\mathrm{O}$ changes to the format of monoclinic material $\mathcal{C}_\mathcal{M}$;
- When $\theta = 90°$, the rotated matrix $\mathbf{C}'_\mathrm{O}$ still keeps the format of orthotropic one $\mathcal{C}_\mathcal{O}$; but note that $\mathbf{C}'_\mathrm{O} \neq \mathbf{C}_\mathrm{O}$ according to the study in [22]. The angle $\theta = 90°$ corresponds to the case that the axis x'_1 is rotated to coincide with the axis x_2 in Fig. 2(a).

The property of the elastic matrix rotation in the last column of Fig. 1 is the basis of the subsequent sections for studying the coupling issue between Lamb and SH waves in a multi-layered composite plate.

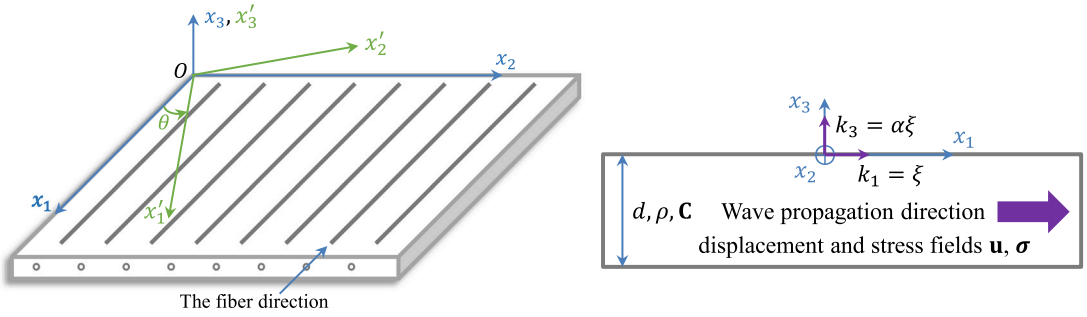

Fig. 2. (a) The schematic of a unidirectional composite lamina, (b) wave propagation model in the lamina.

2.3. Christoffel equation

The guided wave propagating in a lamina is schematically shown in Fig. 2(b), and the wave propagates along the x_1 axis direction. In this condition, the plane-strain state in x_2 direction is implied which leads to the displacement field being invariant to x_2. Thus, the time harmonic displacement equation can be pre-defined in Eq. (7) [1,12].

$$\mathbf{u} = \begin{bmatrix} u_1 \\ u_2 \\ u_3 \end{bmatrix} = \begin{bmatrix} U \\ V \\ W \end{bmatrix} \mathrm{e}^{\mathrm{i}\xi(x_1 + \alpha x_3 - vt)} \tag{7}$$

where, ξ is the wavenumber in x_1 direction and α is the ratio of wavenumbers between x_3 and x_1 direction as shown in Fig. 2(b); v is the phase velocity; U, V, W are the amplitudes of displacements along x_1, x_2, x_3 direction, respectively. Frequency ω can be computed as $\omega = \xi v$.

2.3.1. The coupled Lamb and SH waves in triclinic and monoclinic materials

For general purpose, the elastic matrix of triclinic material $\mathbf{C}_\mathrm{T}$ in Fig. 1 is adopted to derive the Christoffel equation. For other material classes, all the counterparts can be simplified from the corresponding equation of triclinic material. Substituting Eq. (7) into Eqs. (1), (2) and (3), the Christoffel equation for the triclinic material $\mathbf{K}(\alpha)\mathbf{U} = \mathbf{0}$ can be derived in Eq. (8). See [12,22] for the detailed derivation process.

$$\begin{bmatrix} K_{11}(\alpha) & K_{12}(\alpha) & K_{13}(\alpha) \\ K_{12}(\alpha) & K_{22}(\alpha) & K_{23}(\alpha) \\ K_{13}(\alpha) & K_{23}(\alpha) & K_{33}(\alpha) \end{bmatrix} \begin{bmatrix} U \\ V \\ W \end{bmatrix} = \begin{bmatrix} 0 \\ 0 \\ 0 \end{bmatrix} \tag{8}$$

where,

$$\begin{cases} K_{11}(\alpha) = C_{11} - \rho v^2 + 2C_{15}\alpha + C_{55}\alpha^2 \\ K_{22}(\alpha) = C_{66} - \rho v^2 + 2C_{46}\alpha + C_{44}\alpha^2 \\ K_{33}(\alpha) = C_{55} - \rho v^2 + 2C_{35}\alpha + C_{33}\alpha^2 \\ K_{12}(\alpha) = C_{16} + (C_{14} + C_{56})\alpha + C_{45}\alpha^2 \\ K_{13}(\alpha) = C_{15} + (C_{13} + C_{55})\alpha + C_{35}\alpha^2 \\ K_{23}(\alpha) = C_{56} + (C_{36} + C_{45})\alpha + C_{34}\alpha^2 \end{cases} \tag{9}$$

The nontrivial solution of displacement $\mathbf{U}$ in Eq. (8) makes the matrix $\mathbf{K}(\alpha)$ singular, namely $\det\{\mathbf{K}(\alpha)\} = 0$, where $\det\{\cdot\}$ means the operator computing the determinant for a square matrix. The determinant can be derived into a sixth order polynomial equation about α as expressed in Eq. (10), which can be solved by applying a proper numerical algorithm [56].

$$A_6\alpha^6 + A_5\alpha^5 + A_4\alpha^4 + A_3\alpha^3 + A_2\alpha^2 + A_1\alpha + A_0 = 0 \tag{10}$$

where, the seven polynomial coefficients are presented in Appendix A derived by using the software *Mathematica*.

For each root α_r $(r = 1, \ldots, 6)$, there will be a corresponding solution vector of displacement amplitudes $\mathbf{U}_r = [U_r, V_r, W_r]^\mathsf{T}$ based on Eq. (8). For instance, by assigning $U_r = 1$, V_r and W_r are found from the resulted equations as stated in Eq. (11).

$$\begin{cases} U_r = 1 \\ V_r = \frac{K_{11}(\alpha_r)K_{23}(\alpha_r) - K_{12}(\alpha_r)K_{13}(\alpha_r)}{K_{13}(\alpha_r)K_{22}(\alpha_r) - K_{12}(\alpha_r)K_{23}(\alpha_r)} \\ W_r = \frac{K_{11}(\alpha_r)K_{23}(\alpha_r) - K_{12}(\alpha_r)K_{13}(\alpha_r)}{K_{12}(\alpha_r)K_{33}(\alpha_r) - K_{13}(\alpha_r)K_{23}(\alpha_r)} \end{cases} \tag{11}$$

The displacement field $\mathbf{u}$ in Eq. (7) now is written as the superposition of the six solutions in Eq. (12), in which each term within the summation represents a partial wave. Therefore, the denomination partial wave superposition approach (PWSA) is chosen.

$$\begin{cases} u_1 = \left(\sum_{r=1}^{6} \eta_r U_r \mathrm{e}^{\mathrm{i}\xi\alpha_r x_3}\right) \mathrm{e}^{\mathrm{i}\xi(x_1 - vt)} \\ u_2 = \left(\sum_{r=1}^{6} \eta_r V_r \mathrm{e}^{\mathrm{i}\xi\alpha_r x_3}\right) \mathrm{e}^{\mathrm{i}\xi(x_1 - vt)} \\ u_3 = \left(\sum_{r=1}^{6} \eta_r W_r \mathrm{e}^{\mathrm{i}\xi\alpha_r x_3}\right) \mathrm{e}^{\mathrm{i}\xi(x_1 - vt)} \end{cases} \tag{12}$$

where, η_r is the participation factor of a partial wave to be determined. The linear summation form of Eq. (12) can be rearranged to the matrix form of Eq. (13).

$$\underbrace{\begin{bmatrix} u_1 \\ u_2 \\ u_3 \end{bmatrix}}_{\mathbf{u}_{3\times1}} = \underbrace{\begin{bmatrix} U_1 & U_2 & U_3 & U_4 & U_5 & U_6 \\ V_1 & V_2 & V_3 & V_4 & V_5 & V_6 \\ W_1 & W_2 & W_3 & W_4 & W_5 & W_6 \end{bmatrix}}_{\mathbf{U}_{3\times6}} \times \underbrace{\begin{bmatrix} \mathrm{e}^{\mathrm{i}\xi\alpha_1 x_3} & & \\ & \ddots & \\ & & \mathrm{e}^{\mathrm{i}\xi\alpha_6 x_3} \end{bmatrix}}_{\boldsymbol{\Lambda}_{6\times6}(x_3)} \underbrace{\begin{bmatrix} \eta_1 \\ \vdots \\ \eta_6 \end{bmatrix}}_{\boldsymbol{\eta}_{6\times1}} \mathrm{e}^{\mathrm{i}\xi(x_1 - vt)} \tag{13}$$

where, the subscript $m \times n$ designates the matrix dimension.

The PWSA can be also applied to the stress tensor σ_{ij}. Herein, only the three terms σ_{33}, σ_{23}, σ_{13} are extracted in Eq. (14)[2] given that the three terms appertain to the traction free boundary condition that is used to derive dispersion equation in the sequel [12,22].

$$\begin{cases} \sigma_{33} = \left(\sum_{r=1}^{6} \eta_r \beta_{1r} \mathrm{e}^{\mathrm{i}\xi\alpha_r x_3}\right) \mathrm{e}^{\mathrm{i}\xi(x_1 - vt)} \\ \sigma_{23} = \left(\sum_{r=1}^{6} \eta_r \beta_{2r} \mathrm{e}^{\mathrm{i}\xi\alpha_r x_3}\right) \mathrm{e}^{\mathrm{i}\xi(x_1 - vt)} \\ \sigma_{13} = \left(\sum_{r=1}^{6} \eta_r \beta_{3r} \mathrm{e}^{\mathrm{i}\xi\alpha_r x_3}\right) \mathrm{e}^{\mathrm{i}\xi(x_1 - vt)} \end{cases} \tag{14}$$

where, β_{ir} is the amplitude of stress field of a partial wave defined in Eq. (15). Eq. (14) is further rearranged to the matrix form of Eq. (16).

$$\begin{cases} \beta_{1r} = (C_{13} + C_{35}\alpha_r)U_r + (C_{36} + C_{34}\alpha_r)V_r + (C_{35} + C_{33}\alpha_r)W_r \\ \beta_{2r} = (C_{14} + C_{45}\alpha_r)U_r + (C_{46} + C_{44}\alpha_r)V_r + (C_{45} + C_{34}\alpha_r)W_r \\ \beta_{3r} = (C_{15} + C_{55}\alpha_r)U_r + (C_{56} + C_{45}\alpha_r)V_r + (C_{55} + C_{35}\alpha_r)W_r \end{cases} \tag{15}$$

[2] During deriving Eq. (14), a common factor $\mathrm{i}\xi$ is suppressed for the sake of simplicity as adopted in many Refs. [26,54,57].

	Coupled Lamb and SH waves for $\mathbf{C}_{\mathrm{M}}$	Pure Lamb wave for $\mathbf{C}_{\mathrm{O}}$	Pure SH wave for $\mathbf{C}_{\mathrm{O}}$
Christoffel equation	$\begin{bmatrix} K_{11}(\alpha) & K_{12}(\alpha) & K_{13}(\alpha) \\ K_{12}(\alpha) & K_{22}(\alpha) & K_{23}(\alpha) \\ K_{13}(\alpha) & K_{23}(\alpha) & K_{33}(\alpha) \end{bmatrix} \begin{bmatrix} U \\ V \\ W \end{bmatrix} = \begin{bmatrix} 0 \\ 0 \\ 0 \end{bmatrix}$	$\begin{bmatrix} K_{11}(\alpha) & K_{13}(\alpha) \\ K_{13}(\alpha) & K_{33}(\alpha) \end{bmatrix} \begin{bmatrix} U \\ W \end{bmatrix} = \begin{bmatrix} 0 \\ 0 \end{bmatrix}$	$K_{22}(\alpha)\, V = 0$
	$\begin{cases} K_{11}(\alpha) = C_{11} - \rho v^2 + C_{55}\alpha^2 \\ K_{22}(\alpha) = C_{66} - \rho v^2 + C_{44}\alpha^2 \\ K_{33}(\alpha) = C_{55} - \rho v^2 + C_{33}\alpha^2 \\ K_{12}(\alpha) = C_{16} + C_{45}\alpha^2 \\ K_{13}(\alpha) = (C_{13} + C_{55})\alpha \\ K_{23}(\alpha) = (C_{36} + C_{45})\alpha \end{cases}$	$\begin{cases} K_{11}(\alpha) = C_{11} - \rho v^2 + C_{55}\alpha^2 \\ K_{33}(\alpha) = C_{55} - \rho v^2 + C_{33}\alpha^2 \\ K_{13}(\alpha) = (C_{13} + C_{55})\alpha \end{cases}$	$K_{22}(\alpha) = C_{66} - \rho v^2 + C_{44}\alpha^2$
	$A_6\alpha^6 + A_4\alpha^4 + A_2\alpha^2 + A_0 = 0$	$A_4\alpha^4 + A_2\alpha^2 + A_0 = 0$	$A_2\alpha^2 + A_0 = 0$
	$\boldsymbol{\alpha}_{6\times1} = [\alpha_1, -\alpha_1, \alpha_3, -\alpha_3, \alpha_5, -\alpha_5]^{\mathrm{T}}$	$\boldsymbol{\alpha}_{4\times1} = [\alpha_1, -\alpha_1, \alpha_3, -\alpha_3]^{\mathrm{T}}$	$\boldsymbol{\alpha}_{2\times1} = [\alpha_5, -\alpha_5]^{\mathrm{T}}$
	The four polynomial coefficients are presented in Nayfeh's book (1995).	The three polynomial coefficients are presented in Nayfeh's book (1995).	$\begin{cases} A_2 = C_{44} \\ A_0 = C_{66} - \rho v^2 \end{cases}$
Displacement field	$\mathbf{u}_{3\times1} = [u_1, u_2, u_3]^{\mathrm{T}}$ $= \mathbf{U}_{3\times6}\, \boldsymbol{\Lambda}_{6\times6}(x_3)\, \boldsymbol{\eta}_{6\times1} e^{\mathrm{i}\xi(x_1 - vt)}$	$\mathbf{u}_{2\times1} = [u_1, u_3]^{\mathrm{T}}$ $= \mathbf{U}_{2\times4}\, \boldsymbol{\Lambda}_{4\times4}(x_3)\, \boldsymbol{\eta}_{4\times1} e^{\mathrm{i}\xi(x_1 - vt)}$	$\mathbf{u}_{1\times1} = u_2$ $= \mathbf{U}_{1\times2}\, \boldsymbol{\Lambda}_{2\times2}(x_3)\, \boldsymbol{\eta}_{2\times1} e^{\mathrm{i}\xi(x_1 - vt)}$
	$\mathbf{U}_{3\times6} = \begin{bmatrix} U_1 & U_1 & U_3 & U_3 & U_5 & U_5 \\ V_1 & V_1 & V_3 & V_3 & V_5 & V_5 \\ W_1 & -W_1 & W_3 & -W_3 & W_5 & -W_5 \end{bmatrix}$	$\mathbf{U}_{2\times4} = \begin{bmatrix} U_1 & U_1 & U_3 & U_3 \\ W_1 & -W_1 & W_3 & -W_3 \end{bmatrix}$	$\mathbf{U}_{1\times2} = [V_5 \quad V_5]$
	$\boldsymbol{\Lambda}_{6\times6}(x_3) = \begin{bmatrix} e^{\mathrm{i}\xi\alpha_1 x_3} & & \\ & \ddots & \\ & & e^{-\mathrm{i}\xi\alpha_5 x_3} \end{bmatrix}$	$\boldsymbol{\Lambda}_{4\times4}(x_3) = \begin{bmatrix} e^{\mathrm{i}\xi\alpha_1 x_3} & & \\ & \ddots & \\ & & e^{-\mathrm{i}\xi\alpha_3 x_3} \end{bmatrix}$	$\boldsymbol{\Lambda}_{2\times2}(x_3) = \begin{bmatrix} e^{\mathrm{i}\xi\alpha_5 x_3} & \\ & e^{-\mathrm{i}\xi\alpha_5 x_3} \end{bmatrix}$
	$\boldsymbol{\eta}_{6\times1} = [\eta_1, \eta_2, \eta_3, \eta_4, \eta_5, \eta_6]^{\mathrm{T}}$	$\boldsymbol{\eta}_{4\times1} = [\eta_1, \eta_2, \eta_3, \eta_4]^{\mathrm{T}}$	$\boldsymbol{\eta}_{2\times1} = [\eta_5, \eta_6]^{\mathrm{T}}$
Stress field	$\boldsymbol{\sigma}_{3\times1} = [\sigma_{33}, \sigma_{23}, \sigma_{13}]^{\mathrm{T}}$ $= \boldsymbol{\beta}_{3\times6}\, \boldsymbol{\Lambda}_{6\times6}(x_3)\, \boldsymbol{\eta}_{6\times1} e^{\mathrm{i}\xi(x_1 - vt)}$	$\boldsymbol{\sigma}_{2\times1} = [\sigma_{33}, \sigma_{13}]^{\mathrm{T}}$ $= \boldsymbol{\beta}_{2\times4}\, \boldsymbol{\Lambda}_{4\times4}(x_3)\, \boldsymbol{\eta}_{4\times1} e^{\mathrm{i}\xi(x_1 - vt)}$	$\boldsymbol{\sigma}_{1\times1} = \sigma_{23}$ $= \boldsymbol{\beta}_{1\times2}\, \boldsymbol{\Lambda}_{2\times2}(x_3)\, \boldsymbol{\eta}_{2\times1} e^{\mathrm{i}\xi(x_1 - vt)}$
	$\boldsymbol{\beta}_{3\times6} = \begin{bmatrix} \beta_{11} & \beta_{11} & \beta_{13} & \beta_{13} & \beta_{15} & \beta_{15} \\ \beta_{21} & -\beta_{21} & \beta_{23} & -\beta_{23} & \beta_{25} & -\beta_{25} \\ \beta_{31} & -\beta_{31} & \beta_{33} & -\beta_{33} & \beta_{35} & -\beta_{35} \end{bmatrix}$	$\boldsymbol{\beta}_{2\times4} = \begin{bmatrix} \beta_{11} & \beta_{11} & \beta_{13} & \beta_{13} \\ \beta_{31} & -\beta_{31} & \beta_{33} & -\beta_{33} \end{bmatrix}$	$\boldsymbol{\beta}_{1\times2} = [\beta_{25} \quad -\beta_{25}]$
	$\begin{cases} \beta_{1r} = C_{13}U_r + C_{36}V_r + C_{33}\alpha_r W_r \\ \beta_{2r} = C_{45}\alpha_r U_r + C_{44}\alpha_r V_r + C_{45} W_r \\ \beta_{3r} = C_{55}\alpha_r U_r + C_{45}\alpha_r V_r + C_{55} W_r \\ (r = 1,3,5) \end{cases}$	$\begin{cases} \beta_{1r} = C_{13}U_r + C_{33}\alpha_r W_r \\ \beta_{3r} = C_{55}\alpha_r U_r + C_{55} W_r \\ (r = 1,3) \end{cases}$	$\beta_{25} = C_{44}\alpha_5 V_5$

Fig. 3. Christoffel equations, displacement and stress fields of the coupled or pure Lamb and SH waves.

$$\underbrace{\begin{bmatrix} \sigma_{33} \\ \sigma_{23} \\ \sigma_{13} \end{bmatrix}}_{\boldsymbol{\sigma}_{3\times1}} = \underbrace{\begin{bmatrix} \beta_{11} & \beta_{12} & \beta_{13} & \beta_{14} & \beta_{15} & \beta_{16} \\ \beta_{21} & \beta_{22} & \beta_{23} & \beta_{24} & \beta_{25} & \beta_{26} \\ \beta_{31} & \beta_{32} & \beta_{33} & \beta_{34} & \beta_{35} & \beta_{36} \end{bmatrix}}_{\boldsymbol{\beta}_{3\times6}} \times \underbrace{\begin{bmatrix} e^{\mathrm{i}\xi\alpha_1 x_3} & & \\ & \ddots & \\ & & e^{\mathrm{i}\xi\alpha_6 x_3} \end{bmatrix}}_{\boldsymbol{\Lambda}_{6\times6}(x_3)} \underbrace{\begin{bmatrix} \eta_1 \\ \vdots \\ \eta_6 \end{bmatrix}}_{\boldsymbol{\eta}_{6\times1}} e^{\mathrm{i}\xi(x_1 - vt)} \tag{16}$$

It is noteworthy that the Christoffel equation of triclinic material, Eq. (8), leads to the coupled displacement variables among u_1, u_2 and u_3 in Eq. (13), and the coupled stress variables among σ_{33}, σ_{23} and σ_{13} in Eq. (16). This phenomenon characterizes the coupled Lamb and SH waves in the literature [21,51,53].

For monoclinic material, its Christoffel equation can be directly obtained from Eqs. (8) and (9) by making the parameters $C_{14}, C_{15}, C_{24}, C_{25}, C_{34}, C_{35}, C_{46}, C_{56} = 0$. The resulted displacement and stress fields equations $\mathbf{u}_{3\times1}$ and $\boldsymbol{\sigma}_{3\times1}$ are summarized in the first column of Fig. 3 for the sake of conciseness, which still implies the field equations of the coupled Lamb and SH waves with different elements in the matrices $\mathbf{U}_{3\times6}$ and $\boldsymbol{\beta}_{3\times6}$ [12,21,28]. This is the reason that, in the fourth column of Fig. 1, we stipulate $\mathcal{C}_{\mathcal{M}} \subseteq \mathcal{C}_{\mathcal{T}}$ considering that $\mathcal{C}_{\mathcal{M}}$ induces the same property as $\mathcal{C}_{\mathcal{T}}$ in terms of the coupling issue between Lamb and SH waves.

2.3.2. *The pure Lamb and SH waves in orthotropic material*

The Christoffel equation of orthotropic material can be simplified from Eq. (8) by assigning these parameters to be zero, $C_{14}, C_{15}, C_{16}, C_{24}, C_{25}, C_{26}, C_{34}, C_{35}, C_{36}, C_{45}, C_{46}, C_{56} = 0$, which makes the decoupled Christoffel equation, Eqs. (17) and (18). In literature, Eq. (17) produces the field variables of the pure Lamb wave ($u_1, u_3, \sigma_{33}, \sigma_{13}$), and Eq. (18) sets off the field variables of the pure SH wave (u_2, σ_{23}). Their computing formulae already appear in many Refs. [1,12,21,22]. We summarize them in the second and third column of Fig. 3 for brevity. It is evident that the pure Lamb and SH waves are composed with four and two partial waves, respectively. To avoid any confusion, the two partial waves of pure SH mode are numbered as 5 and 6, as implied in the third column of Fig. 3.

$$\begin{bmatrix} C_{11} - \rho v^2 + C_{55}\alpha^2 & (C_{13} + C_{55})\alpha \\ (C_{13} + C_{55})\alpha & C_{55} - \rho v^2 + C_{33}\alpha^2 \end{bmatrix} \begin{bmatrix} U \\ W \end{bmatrix} = \begin{bmatrix} 0 \\ 0 \end{bmatrix} \tag{17}$$

$$(C_{66} - \rho v^2 + C_{44}\alpha^2) V = 0 \tag{18}$$

It should be noted that Eqs. (17) and (18) are directly suitable for transversely isotropic, cubic and isotropic materials. One only needs to substitute the specific elements of elastic matrices of the three materials into Eqs. (17) and (18) to get the corresponding field equations. This is the reason that we stipulate $\mathcal{C}_{\mathcal{TI}}, \mathcal{C}_{\mathcal{C}}, \mathcal{C}_{\mathcal{I}} \subseteq \mathcal{C}_{\mathcal{O}}$ in the fourth column of Fig. 1, since $\mathcal{C}_{\mathcal{TI}}, \mathcal{C}_{\mathcal{C}}, \mathcal{C}_{\mathcal{I}}$ have the same property as $\mathcal{C}_{\mathcal{O}}$ in terms of the pure Lamb and SH waves derived.

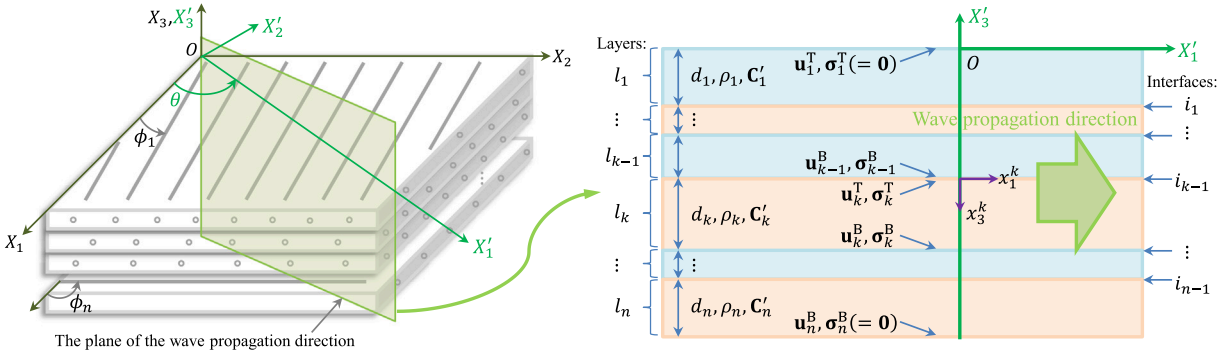

(a) The n-layered laminate model with stacking angles of layups $[\phi_1/\phi_2/\cdots/\phi_n]$

(b) The profile section of the laminate in the wave propagation direction

Fig. 4. Guided wave propagation model in a n-layered composite laminate.

3. Stiffness matrix method

SMM is adopted in this section to derive the dispersion equation of guided waves propagation in arbitrarily stacked composite laminates thanks to its numerical stability and popularity in the academic world [16,27,28].

3.1. The multi-layered composite plate model

We consider a general n-layered laminate with arbitrary stacking angles of layups $[\phi_1/\phi_2/\cdots/\phi_n]$ and the wave propagation direction of interest at angle θ, as illustrated in Fig. 4(a). The profile section of the laminate along the wave propagation direction is cut into Fig. 4(b). For a general layer l_k, its rotation angle becomes $(\theta-\phi_k)$, thus the rotated elastic matrix of this layer becomes $\mathbf{C}_k' = \mathtt{Rot}\{\mathbf{C}_k, \theta-\phi_k\}$, where $\mathbf{C}_k$ is the elastic matrix of layer l_k in its principal direction, and the operator $\mathtt{Rot}\{\cdot,\cdot\}$ is defined in Eq. (5).

According to the study in Sections 2.3.1 and 2.3.2, the different matrix format of $\mathbf{C}_k'$ will lead to different wave type in the layer l_k. If $\mathbf{C}_k'$ is triclinic or monoclinic format, the resulted waves are the coupled Lamb and SH waves in layer l_k (see Section 2.3.1); if $\mathbf{C}_k'$ is orthotropic format, the guided waves are decoupled into the pure Lamb and pure SH waves in layer l_k (see Section 2.3.2). No matter which wave type is considered, the displacement and stress fields in Fig. 3 can be consistently written as Eqs. (19) and (20).

$$\mathbf{u}_{q\times 1} = \mathbf{U}_{q\times p}\boldsymbol{\Lambda}_{p\times p}(x_3)\boldsymbol{\eta}_{p\times 1}\mathrm{e}^{\mathrm{i}\xi(x_1-vt)} \tag{19}$$

$$\boldsymbol{\sigma}_{q\times 1} = \boldsymbol{\beta}_{q\times p}\boldsymbol{\Lambda}_{p\times p}(x_3)\boldsymbol{\eta}_{p\times 1}\mathrm{e}^{\mathrm{i}\xi(x_1-vt)} \tag{20}$$

where, $q = p/2$ and p is the number of partial waves involved in different wave types, specifically, $p=6$ for the coupled Lamb and SH waves, $p=4$ for the pure Lamb wave and $p=2$ for the pure SH wave.

3.2. Lamina stiffness matrix

By tentatively ignoring the matrix dimension of $\mathbf{u}$ and $\boldsymbol{\sigma}$ in Eqs. (19) and (20), the field variables are evaluated at the top side ($x_3^k = 0$ in the local coordinate system) and bottom side ($x_3^k = d_k$) of layer l_k, which results in Eqs. (21) and (22), respectively. Refer to Fig. 4(b) for easy understanding.

$$\begin{cases} \mathbf{u}_k^{\mathrm{T}} = \mathbf{U}_k\boldsymbol{\Lambda}_k(0)\boldsymbol{\eta}_k\mathrm{e}^{\mathrm{i}\xi(x_1-vt)} \\ \boldsymbol{\sigma}_k^{\mathrm{T}} = \boldsymbol{\beta}_k\boldsymbol{\Lambda}_k(0)\boldsymbol{\eta}_k\mathrm{e}^{\mathrm{i}\xi(x_1-vt)} \end{cases} \tag{21}$$

$$\begin{cases} \mathbf{u}_k^{\mathrm{B}} = \mathbf{U}_k\boldsymbol{\Lambda}_k(d_k)\boldsymbol{\eta}_k\mathrm{e}^{\mathrm{i}\xi(x_1-vt)} \\ \boldsymbol{\sigma}_k^{\mathrm{B}} = \boldsymbol{\beta}_k\boldsymbol{\Lambda}_k(d_k)\boldsymbol{\eta}_k\mathrm{e}^{\mathrm{i}\xi(x_1-vt)} \end{cases} \tag{22}$$

where, the subscript k denotes that the associated terms belong to a general layer l_k; the superscript T and B represent the top and bottom side of layer l_k, respectively; d_k is the thickness of layer l_k.

The derivation of SMM starts with collecting the displacement variables at both top and bottom sides into Eq. (23), meanwhile collecting the stress variables at both top and bottom sides into Eq. (24).

$$\begin{bmatrix} \mathbf{u}_k^{\mathrm{T}} \\ \mathbf{u}_k^{\mathrm{B}} \end{bmatrix} = \underbrace{\begin{bmatrix} \mathbf{U}_k\boldsymbol{\Lambda}_k(0) \\ \mathbf{U}_k\boldsymbol{\Lambda}_k(d_k) \end{bmatrix}}_{\boldsymbol{\kappa}_k^u} \boldsymbol{\eta}_k\mathrm{e}^{\mathrm{i}\xi(x_1-vt)} \tag{23}$$

$$\begin{bmatrix} \boldsymbol{\sigma}_k^{\mathrm{T}} \\ \boldsymbol{\sigma}_k^{\mathrm{B}} \end{bmatrix} = \underbrace{\begin{bmatrix} \boldsymbol{\beta}_k\boldsymbol{\Lambda}_k(0) \\ \boldsymbol{\beta}_k\boldsymbol{\Lambda}_k(d_k) \end{bmatrix}}_{\boldsymbol{\kappa}_k^\sigma} \boldsymbol{\eta}_k\mathrm{e}^{\mathrm{i}\xi(x_1-vt)} \tag{24}$$

where, $\boldsymbol{\kappa}_k^u \in \mathbb{C}^{p\times p}$ and $\boldsymbol{\kappa}_k^\sigma \in \mathbb{C}^{p\times p}$ are the lamina matrices of displacement and stress of layer l_k, respectively.

It should be noted that the matrices $\mathbf{U}_k$, $\boldsymbol{\beta}_k$, $\boldsymbol{\Lambda}_k(0)$, $\boldsymbol{\Lambda}_k(d_k)$ may possess different dimensions as manifested in Fig. 3. That makes the lamina matrices $\boldsymbol{\kappa}_k^u$ and $\boldsymbol{\kappa}_k^\sigma$ carry different formats and dimensions for different wave types. To intuitively observe this phenomenon, the formulae computing these lamina matrices corresponding to different wave types are deduced [26,28] and exhibited in Fig. 5.

Eliminating the common term $\boldsymbol{\eta}_k\mathrm{e}^{\mathrm{i}\xi(x_1-vt)}$ in Eqs. (23) and (24) leads to Eq. (25).

$$\begin{bmatrix} \boldsymbol{\sigma}_k^{\mathrm{T}} \\ \boldsymbol{\sigma}_k^{\mathrm{B}} \end{bmatrix} = \underbrace{\boldsymbol{\kappa}_k^\sigma\left(\boldsymbol{\kappa}_k^u\right)^{-1}}_{\boldsymbol{\kappa}_k} \begin{bmatrix} \mathbf{u}_k^{\mathrm{T}} \\ \mathbf{u}_k^{\mathrm{B}} \end{bmatrix} \tag{25}$$

where, $\boldsymbol{\kappa}_k \in \mathbb{C}^{p\times p}$ is defined as the lamina stiffness matrix of layer l_k, and it is usually divided as blocks in Eq. (26).

$$\boldsymbol{\kappa}_k = \begin{bmatrix} \boldsymbol{\kappa}_k^{\mathrm{TT}} & \boldsymbol{\kappa}_k^{\mathrm{TB}} \\ \boldsymbol{\kappa}_k^{\mathrm{BT}} & \boldsymbol{\kappa}_k^{\mathrm{BB}} \end{bmatrix} \tag{26}$$

One should keep in mind that $\boldsymbol{\kappa}_k$ remains the same dimension as $\boldsymbol{\kappa}_k^u$ and $\boldsymbol{\kappa}_k^\sigma$. Specifically, $\boldsymbol{\kappa}_k \in \mathbb{C}^{6\times 6}$ for the coupled Lamb and SH waves, $\boldsymbol{\kappa}_k \in \mathbb{C}^{4\times 4}$ for the pure Lamb wave, and $\boldsymbol{\kappa}_k \in \mathbb{C}^{2\times 2}$ for the pure SH wave.

3.3. Dispersion equation derived from SMM

The lamina stiffness matrix $\boldsymbol{\kappa}_k$ in Eq. (25) plays the role of linking the stress $(\boldsymbol{\sigma}_k^{\mathrm{T}}, \boldsymbol{\sigma}_k^{\mathrm{B}})$ and displacement variables $(\mathbf{u}_k^{\mathrm{T}}, \mathbf{u}_k^{\mathrm{B}})$ at the top and bottom sides of layer l_k. This idea can be generalized to define the *transitional* stiffness matrix $\mathbf{K}_k$ in Eq. (27) that links the stress $(\boldsymbol{\sigma}_1^{\mathrm{T}}, \boldsymbol{\sigma}_k^{\mathrm{B}})$ and

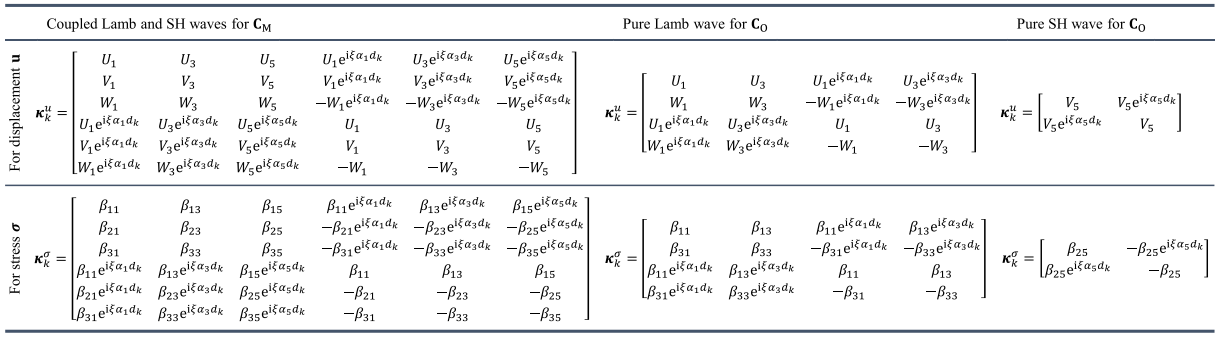

Fig. 5. Lamina matrices of displacement and stress fields for different wave types.

displacement variables $(\mathbf{u}_1^{\mathrm{T}}, \mathbf{u}_k^{\mathrm{B}})$ at the top side of layer l_1 and bottom side of a general layer l_k. Refer to Fig. 4(b) for easy understanding.

$$\begin{bmatrix} \boldsymbol{\sigma}_1^{\mathrm{T}} \\ \boldsymbol{\sigma}_k^{\mathrm{B}} \end{bmatrix} = \underbrace{\begin{bmatrix} \mathbf{K}_k^{\mathrm{TT}} & \mathbf{K}_k^{\mathrm{TB}} \\ \mathbf{K}_k^{\mathrm{BT}} & \mathbf{K}_k^{\mathrm{BB}} \end{bmatrix}}_{\mathbf{K}_k} \begin{bmatrix} \mathbf{u}_1^{\mathrm{T}} \\ \mathbf{u}_k^{\mathrm{B}} \end{bmatrix} \tag{27}$$

In Appendix B, it is proved that $\mathbf{K}_k$ is computed by using Eq. (28). This proof succeeds from some classical references pertaining to SMM [1,15,16,58].

$$\mathbf{K}_k = \begin{bmatrix} \mathbf{K}_{k-1}^{\mathrm{TT}} + \mathbf{K}_{k-1}^{\mathrm{TB}}(\boldsymbol{\kappa}_k^{\mathrm{TT}} - \mathbf{K}_{k-1}^{\mathrm{BB}})^{-1}\mathbf{K}_{k-1}^{\mathrm{BT}} & -\mathbf{K}_{k-1}^{\mathrm{TB}}(\boldsymbol{\kappa}_k^{\mathrm{TT}} - \mathbf{K}_{k-1}^{\mathrm{BB}})^{-1}\boldsymbol{\kappa}_k^{\mathrm{TB}} \\ \boldsymbol{\kappa}_k^{\mathrm{BT}}(\boldsymbol{\kappa}_k^{\mathrm{TT}} - \mathbf{K}_{k-1}^{\mathrm{BB}})^{-1}\mathbf{K}_{k-1}^{\mathrm{BT}} & \boldsymbol{\kappa}_k^{\mathrm{BB}} - \boldsymbol{\kappa}_k^{\mathrm{BT}}(\boldsymbol{\kappa}_k^{\mathrm{TT}} - \mathbf{K}_{k-1}^{\mathrm{BB}})^{-1}\boldsymbol{\kappa}_k^{\mathrm{TB}} \end{bmatrix} \tag{28}$$

where, the matrices $(\boldsymbol{\kappa}_k^{\mathrm{TT}}, \boldsymbol{\kappa}_k^{\mathrm{TB}}, \boldsymbol{\kappa}_k^{\mathrm{BT}}, \boldsymbol{\kappa}_k^{\mathrm{BB}})$ are the block matrices of $\boldsymbol{\kappa}_k$ defined in Eq. (26), and the matrices $(\mathbf{K}_{k-1}^{\mathrm{TT}}, \mathbf{K}_{k-1}^{\mathrm{TB}}, \mathbf{K}_{k-1}^{\mathrm{BT}}, \mathbf{K}_{k-1}^{\mathrm{BB}})$ are the block matrices of $\mathbf{K}_{k-1}$ defined in Eq. (29) characterizing the transitional stiffness matrix from layer l_1 to l_{k-1}.

$$\begin{bmatrix} \boldsymbol{\sigma}_1^{\mathrm{T}} \\ \boldsymbol{\sigma}_{k-1}^{\mathrm{B}} \end{bmatrix} = \underbrace{\begin{bmatrix} \mathbf{K}_{k-1}^{\mathrm{TT}} & \mathbf{K}_{k-1}^{\mathrm{TB}} \\ \mathbf{K}_{k-1}^{\mathrm{BT}} & \mathbf{K}_{k-1}^{\mathrm{BB}} \end{bmatrix}}_{\mathbf{K}_{k-1}} \begin{bmatrix} \mathbf{u}_1^{\mathrm{T}} \\ \mathbf{u}_{k-1}^{\mathrm{B}} \end{bmatrix} \tag{29}$$

Note that $\mathbf{K}_1 = \boldsymbol{\kappa}_1$. Eq. (28) is a recursion formula, which can be evaluated from layer l_2 to the last layer l_n, that finally reaches the *terminative* stiffness matrix $\mathbf{K}_n$ in Eq. (30).

$$\begin{bmatrix} \boldsymbol{\sigma}_1^{\mathrm{T}} \\ \boldsymbol{\sigma}_n^{\mathrm{B}} \end{bmatrix} = \underbrace{\begin{bmatrix} \mathbf{K}_n^{\mathrm{TT}} & \mathbf{K}_n^{\mathrm{TB}} \\ \mathbf{K}_n^{\mathrm{BT}} & \mathbf{K}_n^{\mathrm{BB}} \end{bmatrix}}_{\mathbf{K}_n} \begin{bmatrix} \mathbf{u}_1^{\mathrm{T}} \\ \mathbf{u}_n^{\mathrm{B}} \end{bmatrix} \tag{30}$$

Recall the traction free boundary condition at the top- and bottom-most surfaces of the laminate illustrated in Fig. 4(b), that is $\boldsymbol{\sigma}_1^{\mathrm{T}} = \mathbf{0}$ and $\boldsymbol{\sigma}_n^{\mathrm{B}} = \mathbf{0}$, Eq. (30) evolves to the homogeneous equation in Eq. (31), which finally generates the dispersion equation in Eq. (32) given that the displacement variables $(\mathbf{u}_1^{\mathrm{T}}, \mathbf{u}_n^{\mathrm{B}})$ are non-vanished.

$$\begin{bmatrix} \mathbf{K}_n^{\mathrm{TT}} & \mathbf{K}_n^{\mathrm{TB}} \\ \mathbf{K}_n^{\mathrm{BT}} & \mathbf{K}_n^{\mathrm{BB}} \end{bmatrix} \begin{bmatrix} \mathbf{u}_1^{\mathrm{T}} \\ \mathbf{u}_n^{\mathrm{B}} \end{bmatrix} = \begin{bmatrix} \mathbf{0} \\ \mathbf{0} \end{bmatrix} \tag{31}$$

$$D_S(v, \xi) \triangleq \det \left\{ \begin{vmatrix} \mathbf{K}_n^{\mathrm{TT}} & \mathbf{K}_n^{\mathrm{TB}} \\ \mathbf{K}_n^{\mathrm{BT}} & \mathbf{K}_n^{\mathrm{BB}} \end{vmatrix} \right\} = 0 \tag{32}$$

where, the subscript S denotes that the dispersion equation is built with SMM.

The dispersion equation $D_S(v, \xi) = 0$ can be numerically solved by using bisection method or phase change method [57] to yield the dispersion curves in $v - \xi$, $\omega - \xi$ and $\omega - v$ domains through the relation $\omega = \xi v$. By summarizing the derivation above, we can attain the following three cases corresponding to three wave types.

- If all layers' $\boldsymbol{\kappa}_k \in \mathbb{C}^{6\times6}$, $\mathbf{K}_n \in \mathbb{C}^{6\times6}$ characterizes the coupled Lamb and SH waves in the laminate system.
- If all layers' $\boldsymbol{\kappa}_k \in \mathbb{C}^{4\times4}$, $\mathbf{K}_n \in \mathbb{C}^{4\times4}$ characterizes the pure Lamb wave in the laminate system.
- If all layers' $\boldsymbol{\kappa}_k \in \mathbb{C}^{2\times2}$, $\mathbf{K}_n \in \mathbb{C}^{2\times2}$ characterizes the pure SH wave in the laminate system.

Actually, the three wave types result from the three different formats of laminae's rotated elastic matrices, which are concisely listed in the branch 1 and 2 of Algorithm 1. The pseudo-codes for processing the three wave types are presented in Algorithm 2, 3 and 4, respectively. But before running the three algorithms, Algorithm 1 should be run to determine the correct wave type existing in the laminate system.

Algorithm 1 Judge wave type according to the laminae's rotated elastic matrix format.

Input: Each layer's material properties $(\mathbf{C}_k,\ \rho_k,\ d_k,\ \phi_k)$ for $(k = 1, \ldots, n)$;
The wave propagation angle of interest θ;
The minimum and maximum wavenumber of interest $(\xi_{\min}, \xi_{\max})$;
The minimum, maximum and incremental velocity of interest $(v_{\min}, v_{\max}, \Delta v)$.

1: Compute the rotated elastic matrix $\mathbf{C}'_k$=Rot$\{\mathbf{C}_k, \theta - \phi_k\}$ for $(k = 1, \ldots, n)$.
2: **if** All $\mathbf{C}'_k \in \mathcal{C}_{\mathcal{M}}$ **then** % Branch 1
3: Call Algorithm 2 to process the coupled Lamb and SH waves.
4: **else if** All $\mathbf{C}'_k \in \mathcal{C}_{\mathcal{O}}$ **then** % Branch 2
5: Call Algorithm 3 and 4 to process the pure Lamb and SH waves.
6: **else if** Some $\mathbf{C}'_k \in \mathcal{C}_{\mathcal{M}}$ and other $\mathbf{C}'_k \in \mathcal{C}_{\mathcal{O}}$ **then** % Branch 3
7: Call Algorithm 5 to process the hybrid Lamb and SH waves.
8: **end if**

4. Hybrid matrix strategy

4.1. The incompatibility issue of dimension of lamina matrices

In addition to the three cases inferred at the end of Section 3.3, there is one special case that some layers' $\boldsymbol{\kappa}_k \in \mathbb{C}^{6\times6}$ and other layers' $\boldsymbol{\kappa}_k \in \mathbb{C}^{4\times4}$ or $\boldsymbol{\kappa}_k \in \mathbb{C}^{2\times2}$. For this case, one question is immediately raised out what is the dimension of $\mathbf{K}_n$ and what kind of wave type $\mathbf{K}_n$ characterizes in the whole laminate system? Recalling Eq. (28), there is an implied requirement that all layers' lamina stiffness matrices $\boldsymbol{\kappa}_k$ should have the same dimension $\mathbb{C}^{p\times p}$ in order to proceed the recursion process to produce $\mathbf{K}_n \in \mathbb{C}^{p\times p}$, otherwise the incompatibility issue in terms of the mismatched dimension among the laminae's stiffness matrices is encountered.

Physically, this issue corresponds to the condition that the wave propagation direction of interest in the global coordinate system is just right along the principal direction of one layer (producing the pure

Algorithm 2 Process the coupled Lamb and SH waves via SMM.

Input: Parameters $(\mathbf{C}'_k,\ \rho_k,\ d_k)$ for $(k = 1,\dots,n)$ from Branch 1 of Algorithm 1.

for $v_0 = v_{\min} : \Delta v : v_{\max}$ **do** % Solve the dispersion equation at each fixed v_0.
  for $k = 1:1:n$ **do** % Loop through each layer.
    Compute $(\alpha_r, U_r, V_r, W_r, \beta_{1r}, \beta_{2r}, \beta_{3r})$ for $(r = 1,\dots,6)$ via the first column of Fig. 3 using the data $(\mathbf{C}'_k, \rho_k, v_0)$.
    Compute the lamina matrices $\boldsymbol{\kappa}^u_k, \boldsymbol{\kappa}^\sigma_k \in \mathbb{C}^{6\times6}$ in the first column of Fig. 5.
    Compute the lamina stiffness matrix $\boldsymbol{\kappa}_k \in \mathbb{C}^{6\times6}$ via Eq. (25).
  end for
  Compute the terminative stiffness matrix $\mathbf{K}_n \in \mathbb{C}^{6\times6}$ via Eq. (28) in the recurrent manner.
  Solve $D_S(v_0,\xi) = 0$ in Eq. (32) to get multiple roots $(\xi_1, \xi_2, \dots) \in [\xi_{\min}, \xi_{\max}]$.
end for

Output: All solution points (v_i, ξ_i) in the range $[v_{\min}, v_{\max}] \times [\xi_{\min}, \xi_{\max}]$.

Algorithm 3 Process the pure Lamb wave via SMM.

Input: Parameters $(\mathbf{C}'_k,\ \rho_k,\ d_k)$ for $(k = 1,\dots,n)$ from Branch 2 of Algorithm 1.

for $v_0 = v_{\min} : \Delta v : v_{\max}$ **do** % Solve the dispersion equation at each fixed v_0.
  for $k = 1:1:n$ **do** % Loop through each layer.
    Compute $(\alpha_r, U_r, W_r, \beta_{1r}, \beta_{3r})$ for $(r = 1,\dots,4)$ via the second column of Fig. 3 using the data $(\mathbf{C}'_k, \rho_k, v_0)$.
    Compute the lamina matrices $\boldsymbol{\kappa}^u_k, \boldsymbol{\kappa}^\sigma_k \in \mathbb{C}^{4\times4}$ in the second column of Fig. 5.
    Compute the lamina stiffness matrix $\boldsymbol{\kappa}_k \in \mathbb{C}^{4\times4}$ via Eq. (25).
  end for
  Compute the terminative stiffness matrix $\mathbf{K}_n \in \mathbb{C}^{4\times4}$ via Eq. (28) in the recurrent manner.
  Solve $D_S(v_0,\xi) = 0$ in Eq. (32) to get multiple roots $(\xi_1, \xi_2, \dots) \in [\xi_{\min}, \xi_{\max}]$.
end for

Output: All solution points (v_i, ξ_i) in the range $[v_{\min}, v_{\max}] \times [\xi_{\min}, \xi_{\max}]$.

Algorithm 4 Process the pure SH wave via SMM.

Input: Parameters $(\mathbf{C}'_k,\ \rho_k,\ d_k)$ for $(k = 1,\dots,n)$ from Branch 2 of Algorithm 1.

for $v_0 = v_{\min} : \Delta v : v_{\max}$ **do** % Solve the dispersion equation at each fixed v_0.
  for $k = 1:1:n$ **do** % Loop through each layer.
    Compute $(\alpha_r, V_r, \beta_{2r})$ for $(r = 5,6)$ via the third column of Fig. 3 using the data $(\mathbf{C}'_k, \rho_k, v_0)$.
    Compute the lamina matrices $\boldsymbol{\kappa}^u_k, \boldsymbol{\kappa}^\sigma_k \in \mathbb{C}^{2\times2}$ in the third column of Fig. 5.
    Compute the lamina stiffness matrix $\boldsymbol{\kappa}_k \in \mathbb{C}^{2\times2}$ via Eq. (25).
  end for
  Compute the terminative stiffness matrix $\mathbf{K}_n \in \mathbb{C}^{2\times2}$ via Eq. (28) in the recurrent manner.
  Solve $D_S(v_0,\xi) = 0$ in Eq. (32) to get multiple roots $(\xi_1, \xi_2, \dots) \in [\xi_{\min}, \xi_{\max}]$.
end for

Output: All solution points (v_i, ξ_i) in the range $[v_{\min}, v_{\max}] \times [\xi_{\min}, \xi_{\max}]$.

Algorithm 5 HMS to process the hybrid Lamb and SH waves via SMM.

Input: Parameters $(\mathbf{C}'_k,\ \rho_k,\ d_k)$ for $(k = 1,\dots,n)$ from Branch 3 of Algorithm 1.

for $v_0 = v_{\min} : \Delta v : v_{\max}$ **do** % Solve the dispersion equation at each fixed v_0.
  for $k = 1:1:n$ **do** % Loop through each layer.
    if $\mathbf{C}'_k \in \mathcal{C}_{\mathcal{M}}$ **then** % This layer has the coupled Lamb and SH waves.
      Compute $(\alpha_r, U_r, V_r, W_r, \beta_{1r}, \beta_{2r}, \beta_{3r})$ for $(r = 1,\dots,6)$ via the first column of Fig. 3 using the data $(\mathbf{C}'_k, \rho_k, v_0)$.
      Compute the lamina matrices $\boldsymbol{\kappa}^u_k, \boldsymbol{\kappa}^\sigma_k \in \mathbb{C}^{6\times6}$ in the first column of Fig. 5.
      Compute the lamina stiffness matrix $\boldsymbol{\kappa}_k \in \mathbb{C}^{6\times6}$ via Eq. (25).
    else if $\mathbf{C}'_k \in \mathcal{C}_{\mathcal{O}}$ **then** % This layer has the hybrid Lamb and SH waves.
      Compute $(\alpha_r, U_r, W_r, \beta_{1r}, \beta_{3r})$ for $(r = 1,\dots,4)$ via the second column of Fig. 3 using the data $(\mathbf{C}'_k, \rho_k, v_0)$.
      Compute the lamina matrices $\boldsymbol{\kappa}^u_k, \boldsymbol{\kappa}^\sigma_k \in \mathbb{C}^{4\times4}$ in the second column of Fig. 5.
      Compute $(\alpha_r, V_r, \beta_{2r})$ for $(r = 5,6)$ via the third column of Fig. 3 using the data $(\mathbf{C}'_k, \rho_k, v_0)$.
      Compute the lamina matrices $\boldsymbol{\kappa}^u_k, \boldsymbol{\kappa}^\sigma_k \in \mathbb{C}^{2\times2}$ in the third column of Fig. 5.
      Compute the hybrid lamina matrices $\tilde{\boldsymbol{\kappa}}^u_k \in \mathbb{C}^{6\times6}$ using the obtained $\boldsymbol{\kappa}^u_k \in \mathbb{C}^{4\times4}$ and $\boldsymbol{\kappa}^u_k \in \mathbb{C}^{2\times2}$ based on Eq. (37).
      Compute the hybrid lamina matrices $\tilde{\boldsymbol{\kappa}}^\sigma_k \in \mathbb{C}^{6\times6}$ using the obtained $\boldsymbol{\kappa}^\sigma_k \in \mathbb{C}^{4\times4}$ and $\boldsymbol{\kappa}^\sigma_k \in \mathbb{C}^{2\times2}$ based on Eq. (38).
      Compute the hybrid lamina stiffness matrix $\tilde{\boldsymbol{\kappa}}_k \in \mathbb{C}^{6\times6}$ via Eq. (39).
    end if
  end for
  Compute the hybrid terminative stiffness matrix $\tilde{\mathbf{K}}_n \in \mathbb{C}^{6\times6}$ via Eq. (28) in the recurrent manner.
  Solve $D_S(v_0,\xi) = 0$ in Eq. (32) to get multiple roots $(\xi_1, \xi_2, \dots) \in [\xi_{\min}, \xi_{\max}]$.
end for

Output: All solution points (v_i, ξ_i) in the range $[v_{\min}, v_{\max}] \times [\xi_{\min}, \xi_{\max}]$.

Lamb and SH waves in this layer) but along the off-principal direction of another layer (producing the coupled Lamb and SH waves in that layer). This issue is very common and usually presents in anisotropic composite laminates owing to various stacking angles of layups. However, such a fundamental problem has not been systematically tackled in the literature.

Pant et al. (2014) adopted a pseudo correction measure to circumvent the incompatibility issue. They optionally changed the stacking angles of layups with a minor angle 1° to secure that all layers have the (virtually) coupled Lamb and SH waves [17]. The pseudo correction measure is doable from the numerical way but not orthodox from the mathematical perspective. Barazanchy and Giurgiutiu (2016) proposed an unified method based on eigenvectors sorting and orthogonality principle to bypass the incompatibility issue. But this method was interpreted only for isotropic material, and failed to pass the benchmark test for a 50-layered composite plate [53].

In this paper, we propose a novel hybrid matrix strategy (HMS) to resolve the incompatibility issue, which is effective for various material classes. The most important aspect of HMS is that it is directly derived from the layer-wise PWSA similar to the coupled Lamb and SH waves in Section 2.3.1. Thus, HMS is logically straightforward, mathematically rigorous and numerically stable.

4.2. Hybrid lamina stiffness matrix of pure Lamb and SH waves

The process of deriving HMS is to *re-couple* some layer's $\boldsymbol{\kappa}_k \in \mathbb{C}^{4\times4}$ and $\boldsymbol{\kappa}_k \in \mathbb{C}^{2\times2}$ to yield a hybrid lamina stiffness matrix $\tilde{\boldsymbol{\kappa}}_k \in \mathbb{C}^{6\times6}$, which is compatible with other layer's $\boldsymbol{\kappa}_k \in \mathbb{C}^{6\times6}$ in terms of matrix dimension such that the recursion process in Eq. (28) can be proceeded to produce $\tilde{\mathbf{K}}_n \in \mathbb{C}^{p\times p}$. The displacement fields $\mathbf{u}_{2\times1} = [u_1, u_3]^{\mathrm{T}}$ and $\mathbf{u}_{1\times1} = u_2$ in Fig. 3 can be combined in Eq. (33) for the partial wave superposition form like in Eq. (12).

$$\begin{cases} u_1 = \left(\sum_{r=1}^{4} \eta_r U_r \mathrm{e}^{\mathrm{i}\xi\alpha_r x_3}\right) \mathrm{e}^{\mathrm{i}\xi(x_1 - vt)} \\ u_2 = \left(\sum_{r=5}^{6} \eta_r V_r \mathrm{e}^{\mathrm{i}\xi\alpha_r x_3}\right) \mathrm{e}^{\mathrm{i}\xi(x_1 - vt)} \\ u_3 = \left(\sum_{r=1}^{4} \eta_r W_r \mathrm{e}^{\mathrm{i}\xi\alpha_r x_3}\right) \mathrm{e}^{\mathrm{i}\xi(x_1 - vt)} \end{cases} \tag{33}$$

Rewrite Eq. (33) as the matrix form in Eq. (34).

$$\underbrace{\begin{bmatrix} u_1 \\ u_2 \\ u_3 \end{bmatrix}}_{\mathbf{u}_{3\times1}} = \underbrace{\left[\begin{array}{cccc:cc} U_1 & U_2 & U_3 & U_4 & 0 & 0 \\ 0 & 0 & 0 & 0 & V_5 & V_6 \\ W_1 & W_2 & W_3 & W_4 & 0 & 0 \end{array}\right]}_{\tilde{\mathbf{U}}_{3\times6}} \times \underbrace{\begin{bmatrix} \mathrm{e}^{\mathrm{i}\xi\alpha_1 x_3} & & \\ & \ddots & \\ & & \mathrm{e}^{\mathrm{i}\xi\alpha_6 x_3} \end{bmatrix}}_{\boldsymbol{\Lambda}_{6\times6}(x_3)} \underbrace{\begin{bmatrix} \eta_1 \\ \vdots \\ \eta_6 \end{bmatrix}}_{\boldsymbol{\eta}_{6\times1}} \mathrm{e}^{\mathrm{i}\xi(x_1 - vt)} \tag{34}$$

where, $\tilde{\mathbf{U}}_{3\times6}$ is used to distinguish $\mathbf{U}_{3\times6}$ defined in Fig. 3, and it is regarded as the hybrid version of $\mathbf{U}_{2\times4}$ and $\mathbf{U}_{1\times2}$ in Fig. 3. The tilde '$\sim$' represents the hybrid sense. Physically, the zero elements in $\tilde{\mathbf{U}}_{3\times6}$ indicate the zero amplitudes of the corresponding partial waves.

The stress fields $\boldsymbol{\sigma}_{2\times1} = [\sigma_{33}, \sigma_{13}]^{\mathrm{T}}$ and $\boldsymbol{\sigma}_{1\times1} = \sigma_{23}$ in Fig. 3 can be also combined in Eq. (35) and are further rewritten as the matrix form in Eq. (36).

$$\begin{cases} \sigma_{33} = \left(\sum_{r=1}^{4} \eta_r \beta_{1r} \mathrm{e}^{\mathrm{i}\xi\alpha_r x_3}\right) \mathrm{e}^{\mathrm{i}\xi(x_1 - vt)} \\ \sigma_{23} = \left(\sum_{r=5}^{6} \eta_r \beta_{2r} \mathrm{e}^{\mathrm{i}\xi\alpha_r x_3}\right) \mathrm{e}^{\mathrm{i}\xi(x_1 - vt)} \\ \sigma_{13} = \left(\sum_{r=1}^{4} \eta_r \beta_{3r} \mathrm{e}^{\mathrm{i}\xi\alpha_r x_3}\right) \mathrm{e}^{\mathrm{i}\xi(x_1 - vt)} \end{cases} \tag{35}$$

$$\underbrace{\begin{bmatrix} \sigma_{33} \\ \sigma_{23} \\ \sigma_{13} \end{bmatrix}}_{\boldsymbol{\sigma}_{3\times1}} = \underbrace{\left[\begin{array}{cccc:cc} \beta_{11} & \beta_{12} & \beta_{13} & \beta_{14} & 0 & 0 \\ 0 & 0 & 0 & 0 & \beta_{25} & \beta_{26} \\ \beta_{31} & \beta_{32} & \beta_{33} & \beta_{34} & 0 & 0 \end{array}\right]}_{\tilde{\boldsymbol{\beta}}_{3\times6}} \times \underbrace{\begin{bmatrix} \mathrm{e}^{\mathrm{i}\xi\alpha_1 x_3} & & \\ & \ddots & \\ & & \mathrm{e}^{\mathrm{i}\xi\alpha_6 x_3} \end{bmatrix}}_{\boldsymbol{\Lambda}_{6\times6}(x_3)} \underbrace{\begin{bmatrix} \eta_1 \\ \vdots \\ \eta_6 \end{bmatrix}}_{\boldsymbol{\eta}_{6\times1}} \mathrm{e}^{\mathrm{i}\xi(x_1 - vt)} \tag{36}$$

where, $\tilde{\boldsymbol{\beta}}_{3\times6}$ is used to distinguish $\boldsymbol{\beta}_{3\times6}$ defined in Fig. 3, and it is regarded as the hybrid version of $\boldsymbol{\beta}_{2\times4}$ and $\boldsymbol{\beta}_{1\times2}$ in Fig. 3.

In the hybrid context, the hybrid lamina matrices of displacement and stress of layer l_k can be derived and presented in Eqs. (37) and (38). The derivation is detailed in Appendix C.

$$\tilde{\boldsymbol{\kappa}}_k^{u} = \left[\begin{array}{ccc:ccc} U_1 & U_3 & 0 & U_1\mathrm{e}^{\mathrm{i}\xi\alpha_1 d_k} & U_3\mathrm{e}^{\mathrm{i}\xi\alpha_3 d_k} & 0 \\ 0 & 0 & V_5 & 0 & 0 & V_5\mathrm{e}^{\mathrm{i}\xi\alpha_5 d_k} \\ W_1 & W_3 & 0 & -W_1\mathrm{e}^{\mathrm{i}\xi\alpha_1 d_k} & -W_3\mathrm{e}^{\mathrm{i}\xi\alpha_3 d_k} & 0 \\ \hdashline U_1\mathrm{e}^{\mathrm{i}\xi\alpha_1 d_k} & U_3\mathrm{e}^{\mathrm{i}\xi\alpha_3 d_k} & 0 & U_1 & U_3 & 0 \\ 0 & 0 & V_5\mathrm{e}^{\mathrm{i}\xi\alpha_5 d_k} & 0 & 0 & V_5 \\ W_1\mathrm{e}^{\mathrm{i}\xi\alpha_1 d_k} & W_3\mathrm{e}^{\mathrm{i}\xi\alpha_3 d_k} & 0 & -W_1 & -W_3 & 0 \end{array}\right] \tag{37}$$

$$\tilde{\boldsymbol{\kappa}}_k^{\sigma} = \left[\begin{array}{ccc:ccc} \beta_{11} & \beta_{13} & 0 & \beta_{11}\mathrm{e}^{\mathrm{i}\xi\alpha_1 d_k} & \beta_{13}\mathrm{e}^{\mathrm{i}\xi\alpha_3 d_k} & 0 \\ 0 & 0 & \beta_{25} & 0 & 0 & -\beta_{25}\mathrm{e}^{\mathrm{i}\xi\alpha_5 d_k} \\ \beta_{31} & \beta_{33} & 0 & -\beta_{31}\mathrm{e}^{\mathrm{i}\xi\alpha_1 d_k} & -\beta_{33}\mathrm{e}^{\mathrm{i}\xi\alpha_3 d_k} & 0 \\ \hdashline \beta_{11}\mathrm{e}^{\mathrm{i}\xi\alpha_1 d_k} & \beta_{13}\mathrm{e}^{\mathrm{i}\xi\alpha_3 d_k} & 0 & \beta_{11} & \beta_{13} & 0 \\ 0 & 0 & \beta_{25}\mathrm{e}^{\mathrm{i}\xi\alpha_5 d_k} & 0 & 0 & -\beta_{25} \\ \beta_{31}\mathrm{e}^{\mathrm{i}\xi\alpha_1 d_k} & \beta_{33}\mathrm{e}^{\mathrm{i}\xi\alpha_3 d_k} & 0 & -\beta_{31} & -\beta_{33} & 0 \end{array}\right] \tag{38}$$

The *hybrid* lamina stiffness matrix $\tilde{\boldsymbol{\kappa}}_k$ is computed as Eq. (39) that follows the form of Eq. (25).

$$\tilde{\boldsymbol{\kappa}}_k = \tilde{\boldsymbol{\kappa}}_k^{\sigma} \left(\tilde{\boldsymbol{\kappa}}_k^{u}\right)^{-1} \in \mathbb{C}^{6\times6} \tag{39}$$

It is evident that any two rows of $\tilde{\boldsymbol{\kappa}}_k^{u}$ in Eq. (37) are linearly independent, so being full rank, which secures the numerical stability of HMS. With the compatible lamina stiffness matrices between $\tilde{\boldsymbol{\kappa}}_j, \boldsymbol{\kappa}_i \in \mathbb{C}^{6\times6}$, the *hybrid* terminative stiffness matrix $\tilde{\mathbf{K}}_n \in \mathbb{C}^{6\times6}$ can be computed based on Eq. (28) in the recurrent manner.

The HMS is programmatically interpreted in Algorithm 5, which is logically accompanied by Algorithm 1 to make sure that the current guided wave type correctly corresponds to the hybrid case. Specifically, the branch 3 of Algorithm 1 should be targeted. In correspondence with the HMS, the wave solutions obtained via Algorithm 5 are artificially classified as the *hybrid* Lamb and SH waves to distinguish the terminology of the coupled waves in Algorithm 2 and the pure waves in Algorithm 3 and 4.

5. Numerical validation

5.1. Case of a quasi-isotropic laminate

In this subsection, a carbon-fiber epoxy laminate is used to validate the developed HMS. The laminate consists of eight unidirectional laminae with stacking angles of layups $[0/90/45/-45]_{\mathrm{s}}$, indicating the quasi-isotropic property of this plate. The material properties of the carbon-fiber epoxy lamina are cited from [17] and listed in the following for convenience. This material is commonly used in the aeronautic and aerospace industry. One can check that the elastic matrix $\mathbf{C}$ in Eq. (40) which is along the principal direction of itself belongs to the transversely isotropic class, and thereby orthotropic class.

- Stacking sequence is $[0/90/45/-45]_{\mathrm{s}}$;
- Thickness of each lamina is 0.17 mm;
- Material density is 1650 $\mathrm{kg/m^3}$;
- Elastic matrix $\mathbf{C}$ is presented in Eq. (40).

$$\mathbf{C} = \begin{bmatrix} 145.38 & 3.96 & 3.96 & 0 & 0 & 0 \\ & 10.11 & 3.11 & 0 & 0 & 0 \\ & & 10.11 & 0 & 0 & 0 \\ & & & 3.5 & 0 & 0 \\ & \mathrm{sym} & & & 4.8 & 0 \\ & & & & & 4.8 \end{bmatrix} \mathrm{GPa} \tag{40}$$

The quasi-isotropic stacking sequence of layups results in that there is not a common principal axis among the laminae and thus no pure Lamb or SH waves present in the plate for any propagation angle. For the specific stacking angles $[0/90/45/-45]_{\mathrm{s}}$, when the wave propagation angle of interest just coincides with one layer's private principal direction, i.e. $\theta \in \{0°, 45°, 90°, -45°\}$, the incompatibility issue is just encountered. This subsection demonstrates in detail the HMS to resolve this issue.

5.1.1. The hybrid Lamb and SH waves when $\theta = 0°,\ 45°$ or $90°$

Fig. 6(a) illustrates the process of elastic matrix rotation and the determination of wave type existing in the laminate at the current propagation angle $\theta = 0°$. From the conceptual diagram, it can be seen that, after rotation of Eq. (40), the rotated elastic matrices of the jth layer $\mathbf{C}'_j\,(j = 1,2,7,8)$ belong to the set $\mathcal{C}_{\mathcal{O}}$ but the ith layer $\mathbf{C}'_i\,(i = 3,4,5,6)$ belong to the set $\mathcal{C}_{\mathcal{M}}$. According to the Algorithm 1, branch 3 is targeted that corresponds to the case of the hybrid Lamb and SH waves.

For the rotated $\mathbf{C}'_j \in \mathcal{C}_{\mathcal{O}}$, there exists two kinds of lamina matrices $\boldsymbol{\kappa}^u_j, \boldsymbol{\kappa}^\sigma_j \in \mathbb{C}^{4\times4}$ and $\boldsymbol{\kappa}^u_j, \boldsymbol{\kappa}^\sigma_j \in \mathbb{C}^{2\times2}$ according to the second and third column of Fig. 5, which corresponds to the pure Lamb and SH waves in these layers, respectively. But for another rotated $\mathbf{C}'_i \in \mathcal{C}_{\mathcal{M}}$, they have only the lamina matrices $\boldsymbol{\kappa}^u_i, \boldsymbol{\kappa}^\sigma_i \in \mathbb{C}^{6\times6}$ according to the first column of Fig. 5, corresponding to the coupled Lamb and SH waves in these layers.

Immediately, we are encountering the matrix incompatibility issue between the lamina matrices $\boldsymbol{\kappa}^u_i, \boldsymbol{\kappa}^\sigma_i \in \mathbb{C}^{6\times6}$, $\boldsymbol{\kappa}^u_j, \boldsymbol{\kappa}^\sigma_j \in \mathbb{C}^{4\times4}$ and $\boldsymbol{\kappa}^u_j, \boldsymbol{\kappa}^\sigma_j \in \mathbb{C}^{2\times2}$. The HMS developed in Section 4 is devoted to resolve this issue, which is achieved by reconstructing $\boldsymbol{\kappa}^u_j \in \mathbb{C}^{4\times4}, \boldsymbol{\kappa}^u_j \in \mathbb{C}^{2\times2}$ to the hybrid matrix $\tilde{\boldsymbol{\kappa}}^u_j \in \mathbb{C}^{6\times6}$ based on Eq. (41), meanwhile, reconstructing $\boldsymbol{\kappa}^\sigma_j \in \mathbb{C}^{4\times4}, \boldsymbol{\kappa}^\sigma_j \in \mathbb{C}^{2\times2}$ to another hybrid matrix $\tilde{\boldsymbol{\kappa}}^\sigma_j \in \mathbb{C}^{6\times6}$ based on Eq. (42).

$$\left(\boldsymbol{\kappa}^u_j \in \mathbb{C}^{4\times4}, \boldsymbol{\kappa}^u_j \in \mathbb{C}^{2\times2}\right) \xrightarrow{\text{Eq. (37)}} \tilde{\boldsymbol{\kappa}}^u_j \in \mathbb{C}^{6\times6} \tag{41}$$

$$\left(\boldsymbol{\kappa}^\sigma_j \in \mathbb{C}^{4\times4}, \boldsymbol{\kappa}^\sigma_j \in \mathbb{C}^{2\times2}\right) \xrightarrow{\text{Eq. (38)}} \tilde{\boldsymbol{\kappa}}^\sigma_j \in \mathbb{C}^{6\times6} \tag{42}$$

Then, the hybrid matrices $\tilde{\boldsymbol{\kappa}}^u_j, \tilde{\boldsymbol{\kappa}}^\sigma_j \in \mathbb{C}^{6\times6}$ are used to compute the hybrid lamina stiffness matrix $\tilde{\boldsymbol{\kappa}}_j \in \mathbb{C}^{6\times6}\,(j = 1,2,7,8)$ based on Eq. (39), which is compatible to the lamina stiffness matrix $\boldsymbol{\kappa}_i \in \mathbb{C}^{6\times6}\,(i = 3,4,5,6)$ obtained from Eq. (25) for $\boldsymbol{\kappa}^u_i, \boldsymbol{\kappa}^\sigma_i \in \mathbb{C}^{6\times6}$. To this step, all layers' lamina stiffness matrices are now compatible and they are assembled together to yield the hybrid terminative stiffness matrix $\tilde{\mathbf{K}}_8 \in \mathbb{C}^{6\times6}$ in the recurrent manner based on Eq. (28).

The elaborated process above has been vividly illustrated in the last two columns of Fig. 6(a). Furthermore, it is logically and programmatically encrypted in Algorithm 1 and 5. The computed dispersion curves of the hybrid Lamb and SH waves are depicted in Fig. 7(a) corresponding to the current propagation angle $\theta = 0°$.

The incompatibility issue is still occurring at $\theta = \pm45°$ and $90°$ due to the stacking angles of layups $[0/90/45/-45]_s$, and it can be qualitatively analyzed akin to the conceptual diagram of $\theta = 0°$ in Fig. 6(a). To avoid redundancy, we only illustrate the angle $\theta = 45°$ in Fig. 6(c). It shows that, after rotation, the elastic matrices of the 3rd to the 6th layer keep the orthotropic format, i.e. $\mathbf{C}'_j \in \mathcal{C}_{\mathcal{O}}\,(j = 3,4,5,6)$, which is conjugated with Fig. 6(a) in the graphical sense. Thus, the HMS should be applied to these layers. After running Algorithm 1 and 5, the dispersion curves of the hybrid Lamb and SH waves are depicted in Fig. 7(c) and (d) for $\theta = 45°$ and $\theta = 90°$, respectively.

5.1.2. The coupled Lamb and SH waves when $\theta = 30°$

When the wave direction of interest does not coincide with any principal axis of all layers, i.e. $\theta \notin \{0°, 45°, 90°, -45°\}$, the rotated $\mathbf{C}'_i$ of all layers shall belong to the set $\mathcal{C}_{\mathcal{M}}$, which gives rise to the unified lamina stiffness matrix $\boldsymbol{\kappa}_i \in \mathbb{C}^{6\times6}\,(i = 1,\ldots,8)$ between all layers according to the branch 1 of Algorithm 1. Here, we take a typical angle $\theta = 30°$ to present the process of determining the coupled type of Lamb and SH waves as illustrated in Fig. 6(b). For the coupled case, Algorithm 2 should be adopted to compute the dispersion solutions. After computation, the dispersion curves of the coupled Lamb and SH waves are depicted in Fig. 7(b) for the current angle $\theta = 30°$.

Note that the experimental data points in Fig. 7 are extracted from [17], and they are used in Fig. 7 for the comparison purpose from the experimental perspective. The good agreement between the theoretically computed curves and the experimental data points shown in Fig. 7, as a consequence, validates the feasibility and effectiveness of the combined SMM and HMS methodology.

If a certain wave propagation angle θ leads to the incompatibility issue, we artificially define this angle as the *singular angle* of the laminate. To intuitively observe all the singular angles of the quasi-isotropic laminate, the polar plot of wave velocities are created in Fig. 8 for $fd = 0.1$ MHz mm and $fd = 0.4$ MHz mm. In this figure, the eight singular angles are indicated, they are $\theta \in \{0°, 45°, 90°, 135°, 180°, 225°, 270°, 315°\}$.

5.1.3. Illustration of the pseudo correction measure

Pant's pseudo correction measure to alleviate the incompatibility issue is presented in [17]. We conceptually illustrate it in Fig. 9 for the angle $\theta = 0°$ which has been discussed in Fig. 6(a) using the HMS. The core idea of this measure is detailed in the right-most two columns of Fig. 9. By additionally rotating the $\mathbf{C}'_j \in \mathcal{C}_{\mathcal{O}}\,(j = 1,2,7,8)$ with a minor angle $\Delta\theta = -1°$, all the rotated elastic matrices now belong to the set $\mathcal{C}_{\mathcal{M}}$ that produces the (virtually) coupled Lamb and SH waves.

As $\Delta\theta = -1°$ is relatively small, this pseudo correction has very little effect on the overall stiffness of the laminate. Thus, it is doable from the numerical way but not orthodox from the mathematical viewpoint. In metallic-composite laminates, this pseudo correction measure is invalid since the elastic matrix of the metallic layer always remains the isotropic format irrespective of the rotation angle. We will demonstrate this case in Section 5.2.3.

5.2. Case of a metallic-composite laminate

In this subsection, HMS is applied to a metallic-composite laminate composed of three aluminum layers and four glass fiber layers with stacking angles of layups [Al/0/90/Al/90/0/Al], where Al means the aluminum layer. The material properties of the two materials are cited from [17] and listed in the following for convenience. Thanks to the isotropic property of aluminum material, there exist two common principal axes between the aluminum and glass fiber layers at 0° and 90°.

- Stacking sequence is [Al/0/90/Al/90/0/Al];
- Ply thicknesses of aluminum and glass fiber layers are 0.33 mm and 0.127 mm, respectively;
- Densities of aluminum and glass fiber are 2780 $\mathrm{kg/m^3}$ and 1980 $\mathrm{kg/m^3}$, respectively;
- Elastic matrices of aluminum and glass fiber along their respective principal axis direction are $\mathbf{C}_{\mathrm{Al}}$ of Eq. (43) and $\mathbf{C}_{\mathrm{GF}}$ of Eq. (44);
- The set relation is $\mathbf{C}_{\mathrm{Al}} \in \mathcal{C}_{\mathcal{I}}$ and $\mathbf{C}_{\mathrm{GF}} \in \mathcal{C}_{\mathcal{TI}} \subseteq \mathcal{C}_{\mathcal{O}}$.

$$\mathbf{C}_{\mathrm{Al}} = \begin{bmatrix} 108.31 & 53.35 & 53.35 & 0 & 0 & 0 \\ & 108.31 & 53.35 & 0 & 0 & 0 \\ & & 108.31 & 0 & 0 & 0 \\ & & & 27.48 & 0 & 0 \\ & & & & 27.48 & 0 \\ & \mathrm{sym} & & & & 27.48 \end{bmatrix} \mathrm{GPa} \tag{43}$$

$$\mathbf{C}_{\mathrm{GF}} = \begin{bmatrix} 53.77 & 4.95 & 4.95 & 0 & 0 & 0 \\ & 11.49 & 3.99 & 0 & 0 & 0 \\ & & 11.49 & 0 & 0 & 0 \\ & & & 3.75 & 0 & 0 \\ & & & & 3.70 & 0 \\ & \mathrm{sym} & & & & 3.70 \end{bmatrix} \mathrm{GPa} \tag{44}$$

5.2.1. The pure Lamb and SH waves when $\theta = 0°$ or $90°$

Fig. 10(a) illustrates the process of determining wave type when one principal axis direction $\theta = 0°$ is concerned. At this direction, the rotated elastic matrices of aluminum layers remain the isotropic

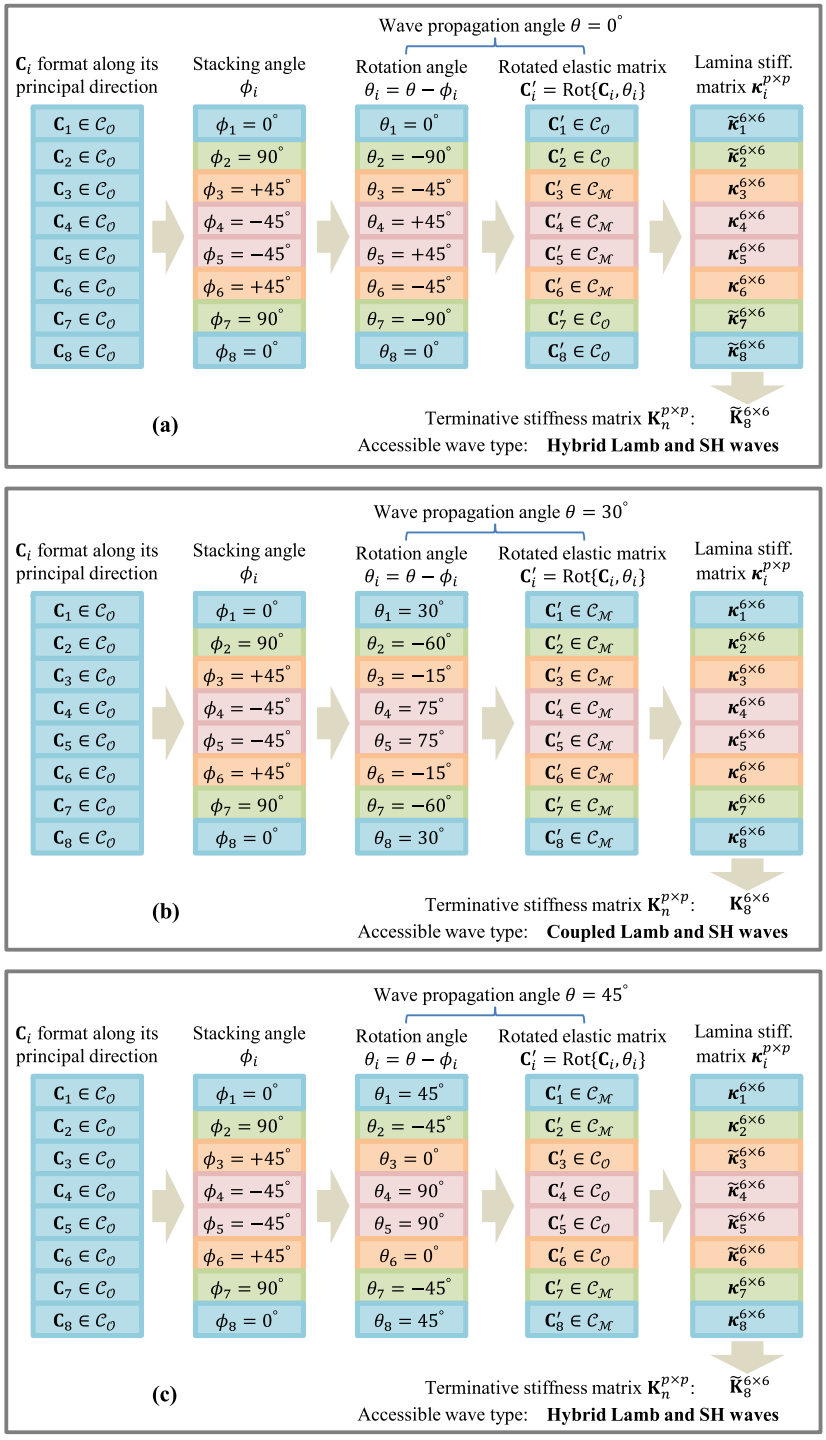

Fig. 6. Conceptual diagram of determining the wave type existing in the quasi-isotropic laminate $[0/90/45/-45]_s$ at the wave propagation angle (a) $\theta = 0°$, (b) $\theta = 30°$, (c) $\theta = 45°$.

property $\mathbf{C}_i' \in C_\mathcal{I}$ $(i = 1, 4, 7)$, and the rotated elastic matrices of glass fiber layers keep the orthotropic property $\mathbf{C}_j' \in C_\mathcal{O}$ $(j = 2, 3, 5, 6)$. Recall the set relation $C_\mathcal{I} \subseteq C_\mathcal{O}$ in Fig. 1, we can also dictate $\mathbf{C}_i' \in C_\mathcal{O}$ $(i = 1, 4, 7)$. As such, all the rotated elastic matrices now belong to the orthotropic class that finally produces the pure Lamb and SH waves present in each lamina, thereby in the whole laminate, for the specific angle $\theta = 0°$. For another principal axis direction $\theta = 90°$, the same outcome of the pure case can be anticipated. The dispersion curves of the pure Lamb and SH waves at the two principal axes directions are retrieved in Fig. 11(a)(e) after running Algorithm 1, 3 and 4. The good agreement between the computed curves and the experimental data points certifies the high accuracy of SMM in processing the pure waves of the metallic-composite laminate.

5.2.2. The hybrid Lamb and SH waves when $\theta = 20°$, $45°$ or $70°$

There are many singular angles that invoke the incompatibility issue in the metallic-composite laminate. Fig. 10(b) illustrates the process of determining wave type when $\theta = 45°$. At this direction, the elastic matrices of aluminum layers are rotated to $\mathbf{C}_i' \in C_\mathcal{I} \subseteq C_\mathcal{O}$ $(i = 1, 4, 7)$ due to the rotation invariance property of isotropic material, whereas the elastic matrices of the glass fiber layers are rotated to

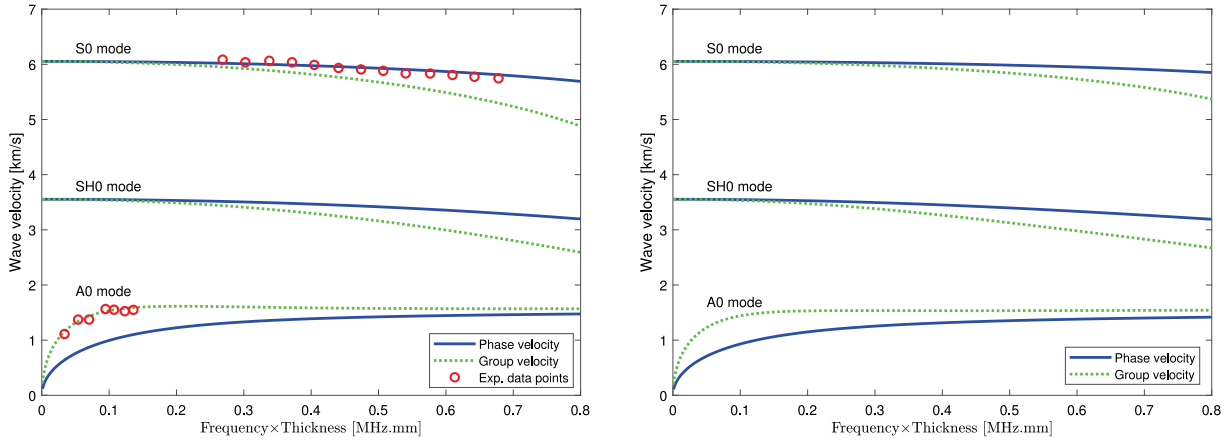

(a) $\theta = 0°$, the hybrid case (b) $\theta = 30°$, the coupled case

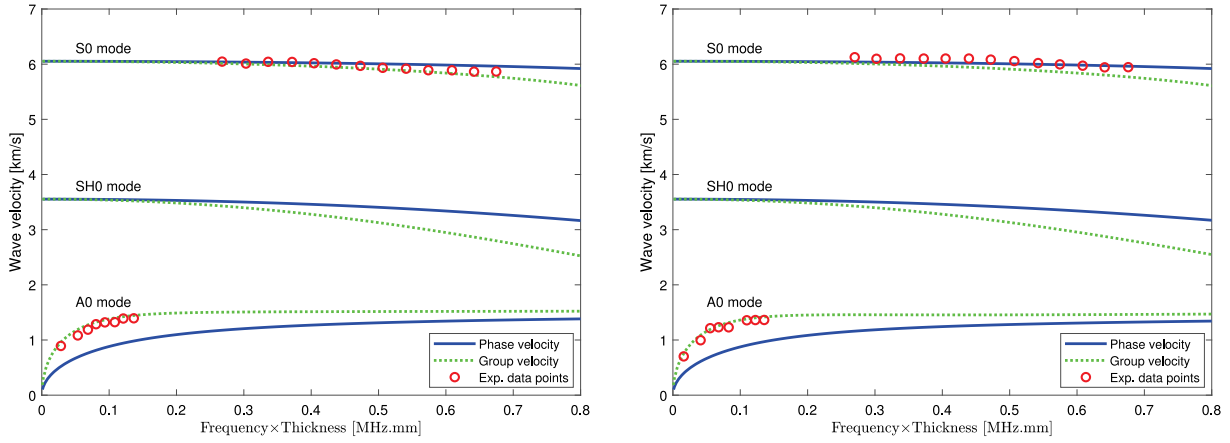

(c) $\theta = 45°$, the hybrid case (d) $\theta = 90°$, the hybrid case

Fig. 7. Dispersion curves of the hybrid or coupled Lamb and SH waves of the quasi-isotropic laminate. The experimental data points are extracted from [17].

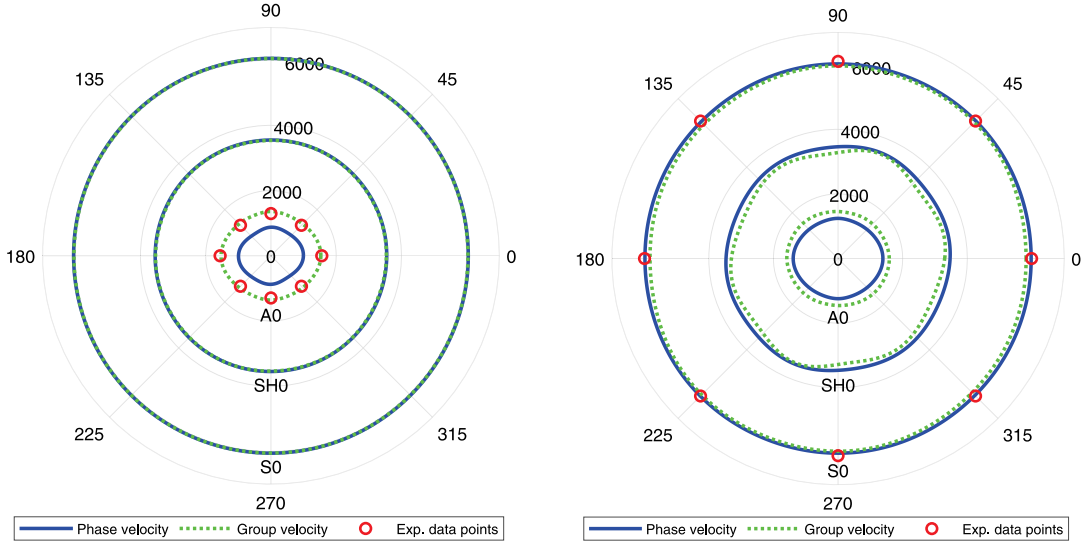

(a) $fd = 0.1\,\mathrm{MHz}\cdot\mathrm{mm}$ (b) $fd = 0.4\,\mathrm{MHz}\cdot\mathrm{mm}$

Fig. 8. Polar plot of wave velocity (unit: m/s). Eight singular angles $\theta \in \{0°, 45°, 90°, 135°, 180°, 225°, 270°, 315°\}$ present in the quasi-isotropic laminate. The experimental data points are extracted from [17].

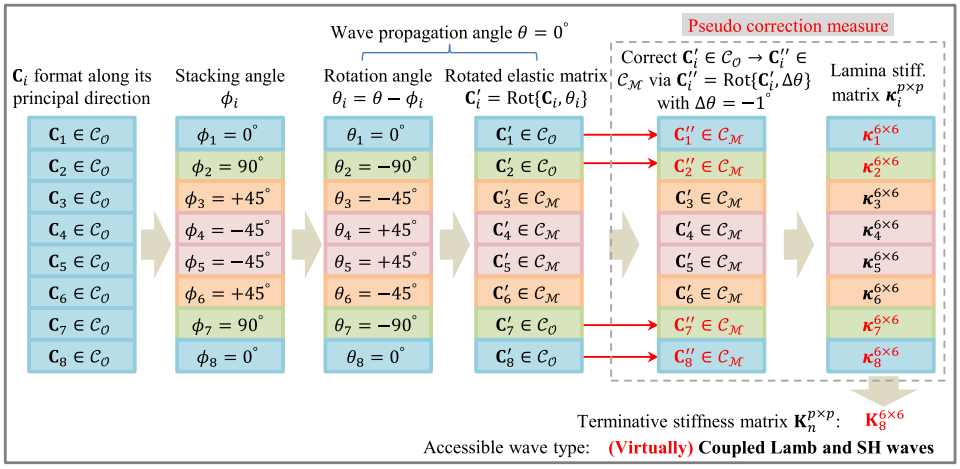

Fig. 9. Conceptual diagram of pseudo correction measure to deal with the incompatibility issue of the quasi-isotropic laminate when $\theta = 0^\circ$.

$\mathbf{C}'_j \in \mathcal{C}_\mathcal{M}\,(j = 2,3,5,6)$. The inconformity of elastic matrix classes between aluminum and glass fiber layers at the current angle $\theta = 45^\circ$ makes the requirement that only the hybrid $\tilde{\boldsymbol{\kappa}}_i \in \mathbb{C}^{6\times6}\,(i = 1,4,7)$ of the aluminum layers are compatible with the $\boldsymbol{\kappa}_j \in \mathbb{C}^{6\times6}\,(j = 2,3,5,6)$ of the glass fiber layers as illustrated in Fig. 10(b). Correspondingly, the hybrid type of Lamb and SH waves is determined according to the branch 3 of Algorithm 1. For another two angles $\theta = 20^\circ$ and 70°, the same hybrid wave type can be analyzed. After running Algorithm 5, the dispersion curves at the three angles $\theta = 20^\circ, 45^\circ, 70^\circ$ are retrieved in Fig. 11(b), (c), (d), respectively. The reason of exhibiting the dispersion curves of $\theta = 20^\circ$ and 70° in Fig. 11 is that the experimental data of the two angles are available from [17]. The good agreement between the computed curves and the experimental data points validates the feasibility of HMS in processing the metallic-composite laminate.

In the quasi-isotropic laminate $[0/90/45/-45]_\mathrm{s}$ of Section 5.1, there are only eight singular angles $\theta \in \{0^\circ, 45^\circ, 90^\circ, 135^\circ, 180^\circ, 225^\circ, 270^\circ, 315^\circ\}$ as implied in Fig. 8. However, in the metallic-composite laminate, any propagation angle is singular except $\theta \in \{0^\circ, 90^\circ, 180^\circ, 270^\circ\}$. This is the major difference between the polar plot of the quasi-isotropic laminate in Fig. 8 and the polar plot of the metallic-composite laminate in Fig. 12.

5.2.3. Superiority of HMS over the pseudo correction measure

Fig. 10(c) illustrates the ineffectiveness of pseudo correction measure for processing the incompatibility issue of metallic-composite laminate. It shows that the additionally rotated elastic matrices of aluminum layers still remains isotropic property, $\mathbf{C}''_i \in \mathcal{C}_\mathcal{I}\,(i = 1,4,7)$, due to the rotation invariance of isotropic material. In consequence, the two kinds of lamina stiffness matrices of aluminum layers $\left(\boldsymbol{\kappa}_i \in \mathbb{C}^{4\times4}, \boldsymbol{\kappa}_i \in \mathbb{C}^{2\times2}\right)$ $(i = 1,4,7)$ are still incompatible with the $\boldsymbol{\kappa}_j \in \mathbb{C}^{6\times6}\,(j = 2,3,5,6)$ of glass fiber layers if without using the hybrid ones $\tilde{\boldsymbol{\kappa}}_i \in \mathbb{C}^{6\times6}\,(i = 1,4,7)$ employed in Fig. 10(b). This illustration proves that pseudo correction measure fails to deal with the incompatibility issue of metallic-composite laminate, while HMS is the effective solution to address this issue.

6. Discussion

6.1. Lamina stiffness matrix of triclinic material

To apply SMM to triclinic material, the lamina matrices of displacement and stress of this material is reported in Eqs. (45) and (46)[3] whose derivation starts with Eqs. (12) and (14) and follows the procedures of Fig. C.13. As such, the lamina stiffness matrix of triclinic material can be computed by $\boldsymbol{\kappa}_k^{\mathcal{T}} = \boldsymbol{\kappa}_k^{\sigma}\left(\boldsymbol{\kappa}_k^{u}\right)^{-1} \in \mathbb{C}^{6\times6}$ based on Eq. (25), where the superscript $\mathcal{T}$ denotes the triclinic material. In this case, $\boldsymbol{\kappa}_k^{\mathcal{T}} \in \mathbb{C}^{6\times6}$ is compatible with $\boldsymbol{\kappa}_k^{6\times6}$ of monoclinic material and the hybrid $\tilde{\boldsymbol{\kappa}}_k^{6\times6}$. This fact makes the SMM-HMS framework be able to deal with guided waves propagation in the most inhomogeneous composite plates that are made up of the simplest isotropic, commonly used orthotropic and fully anisotropic triclinic materials.

$$\boldsymbol{\kappa}_k^{u} = \left[\begin{array}{ccc:ccc} U_1 & U_3 & U_5 & U_2\mathrm{e}^{-\mathrm{i}\xi\alpha_2 d_k} & U_4\mathrm{e}^{-\mathrm{i}\xi\alpha_4 d_k} & U_6\mathrm{e}^{-\mathrm{i}\xi\alpha_6 d_k} \\ V_1 & V_3 & V_5 & V_2\mathrm{e}^{-\mathrm{i}\xi\alpha_2 d_k} & V_4\mathrm{e}^{-\mathrm{i}\xi\alpha_4 d_k} & V_6\mathrm{e}^{-\mathrm{i}\xi\alpha_6 d_k} \\ W_1 & W_3 & W_5 & W_2\mathrm{e}^{-\mathrm{i}\xi\alpha_2 d_k} & W_4\mathrm{e}^{-\mathrm{i}\xi\alpha_4 d_k} & W_6\mathrm{e}^{-\mathrm{i}\xi\alpha_6 d_k} \\ \hdashline U_1\mathrm{e}^{\mathrm{i}\xi\alpha_1 d_k} & U_3\mathrm{e}^{\mathrm{i}\xi\alpha_3 d_k} & U_5\mathrm{e}^{\mathrm{i}\xi\alpha_5 d_k} & U_2 & U_4 & U_6 \\ V_1\mathrm{e}^{\mathrm{i}\xi\alpha_1 d_k} & V_3\mathrm{e}^{\mathrm{i}\xi\alpha_3 d_k} & V_5\mathrm{e}^{\mathrm{i}\xi\alpha_5 d_k} & V_2 & V_4 & V_6 \\ W_1\mathrm{e}^{\mathrm{i}\xi\alpha_1 d_k} & W_3\mathrm{e}^{\mathrm{i}\xi\alpha_3 d_k} & W_5\mathrm{e}^{\mathrm{i}\xi\alpha_5 d_k} & W_2 & W_4 & W_6 \end{array}\right] \tag{45}$$

$$\boldsymbol{\kappa}_k^{\sigma} = \left[\begin{array}{ccc:ccc} \beta_{11} & \beta_{13} & \beta_{15} & \beta_{12}\mathrm{e}^{-\mathrm{i}\xi\alpha_2 d_k} & \beta_{14}\mathrm{e}^{-\mathrm{i}\xi\alpha_4 d_k} & \beta_{16}\mathrm{e}^{-\mathrm{i}\xi\alpha_6 d_k} \\ \beta_{21} & \beta_{23} & \beta_{25} & \beta_{22}\mathrm{e}^{-\mathrm{i}\xi\alpha_2 d_k} & \beta_{24}\mathrm{e}^{-\mathrm{i}\xi\alpha_4 d_k} & \beta_{26}\mathrm{e}^{-\mathrm{i}\xi\alpha_6 d_k} \\ \beta_{31} & \beta_{33} & \beta_{35} & \beta_{32}\mathrm{e}^{-\mathrm{i}\xi\alpha_2 d_k} & \beta_{34}\mathrm{e}^{-\mathrm{i}\xi\alpha_4 d_k} & \beta_{36}\mathrm{e}^{-\mathrm{i}\xi\alpha_6 d_k} \\ \hdashline \beta_{11}\mathrm{e}^{\mathrm{i}\xi\alpha_1 d_k} & \beta_{13}\mathrm{e}^{\mathrm{i}\xi\alpha_3 d_k} & \beta_{15}\mathrm{e}^{\mathrm{i}\xi\alpha_5 d_k} & \beta_{12} & \beta_{14} & \beta_{16} \\ \beta_{21}\mathrm{e}^{\mathrm{i}\xi\alpha_1 d_k} & \beta_{23}\mathrm{e}^{\mathrm{i}\xi\alpha_3 d_k} & \beta_{25}\mathrm{e}^{\mathrm{i}\xi\alpha_5 d_k} & \beta_{22} & \beta_{24} & \beta_{26} \\ \beta_{31}\mathrm{e}^{\mathrm{i}\xi\alpha_1 d_k} & \beta_{33}\mathrm{e}^{\mathrm{i}\xi\alpha_3 d_k} & \beta_{35}\mathrm{e}^{\mathrm{i}\xi\alpha_5 d_k} & \beta_{32} & \beta_{34} & \beta_{36} \end{array}\right] \tag{46}$$

6.2. HMS in cross-ply laminate and sandwich plate

In Fig. 10(a), we can further recast each layer's $\boldsymbol{\kappa}_i^{4\times4}$, $\boldsymbol{\kappa}_i^{2\times2}$ into $\tilde{\boldsymbol{\kappa}}_i^{6\times6}\,(i = 1,\ldots,7)$ based on Eqs. (41) and (42). As such, the hybrid $\tilde{\mathbf{K}}_7^{6\times6}$ is computed, which simultaneously characterizes the pure Lamb and SH waves. This tactful manipulation is very useful for handling cross-ply laminate, e.g. the woven fabric panel $[0/90]_3$ in [59], where the two principal directions $\theta = 0^\circ$ and 90° produce the pure Lamb and SH waves that can be simultaneously processed via HMS to reduce computational time. In this sense, HMS is an unified approach able to process the pure case in addition to the hybrid one.

[3] During deriving Eqs. (45) and (46), all the six partial waves' solutions of triclinic material have to be undertaken, since there is no the pair relation of α^2 in Eq. (10) like the counterpart of monoclinic material.

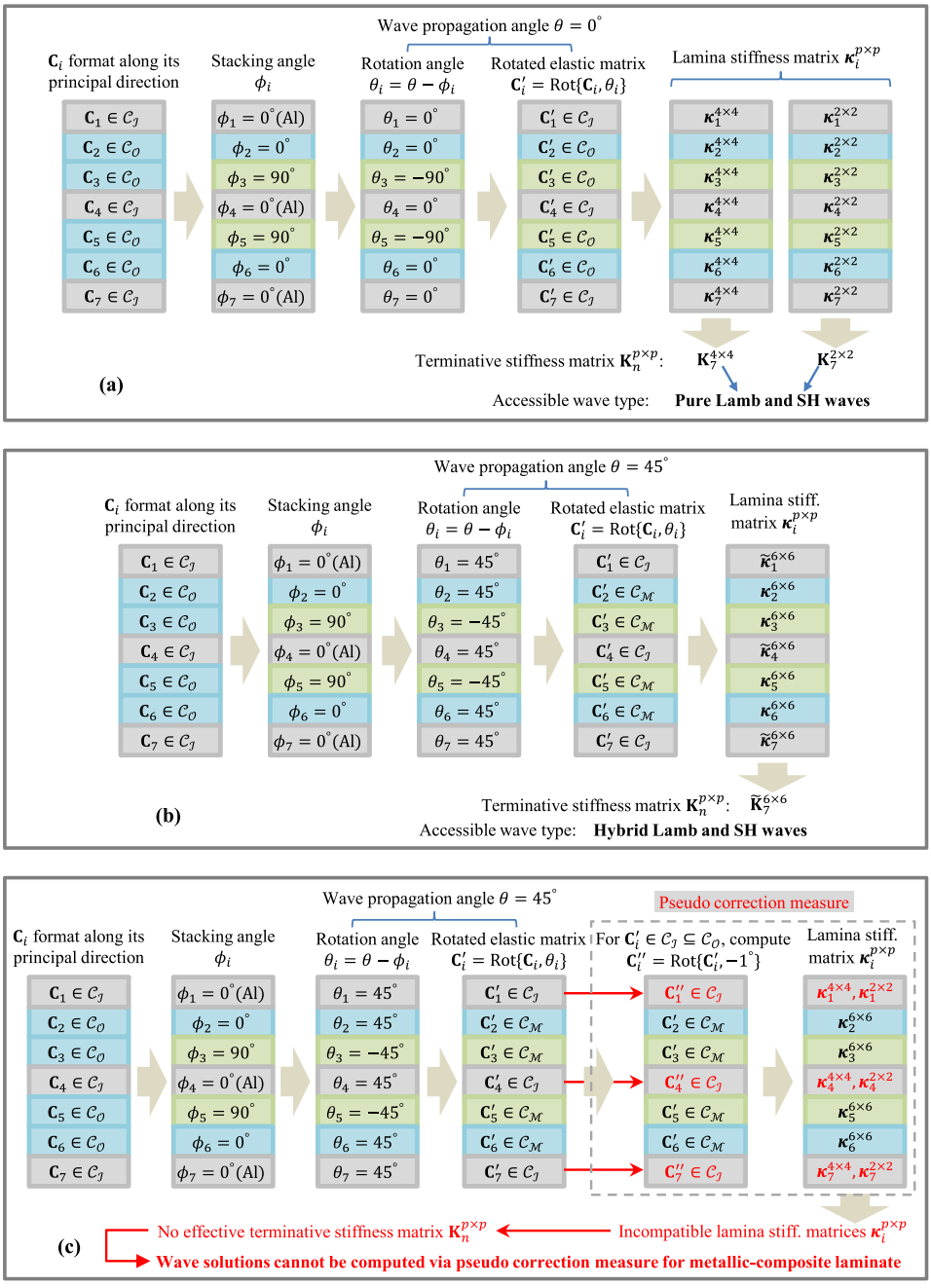

Fig. 10. Conceptual diagram of determining the wave type existing in the metallic-composite laminate [Al/0/90/Al/90/0/Al] at the wave propagation angle (a) $\theta = 0°$, (b) $\theta = 45°$ and (c) $\theta = 45°$ for pseudo correction measure.

Multi-layered sandwich plate is generally made up of arbitrarily oriented CFRP skins and aluminum alloy honeycomb core, where the core layer is considered as isotropic material. For instance, the IFS plate of A380 nacelle in [60] having stacking angles [0/-45/45/0/Al/0/45/-45/0]. For such a complex structure, when $\theta = 0°$, both the honeycomb core and the 0° CFRP layers should be handled with HMS. This case is different from Fig. 10(b) where the hybrid manipulation is conducted only for aluminum layers. Using the conceptual diagram to determine which layers should be manipulated via HMS is intuitional but cumbersome. The developed Algorithm 1 and 5, however, can automatically identify the singular angles and deploy the peculier layers need to be handled with HMS. This fact shows the practical value of HMS that it is able to handle the arbitrarily oriented multi-layered sandwich plate which is widely used in aeronautic and aerospace industry.

6.3. Comparison between SMM-HMS and other methods

The TMM and GMM versions of HMS were established in [22]. Different from the counterpart of SMM, the hybridization of the pure Lamb and SH waves in TMM and GMM is directly exerted on $\tilde{\mathbf{U}}_{3\times6}$ of Eq. (34) and $\tilde{\boldsymbol{\beta}}_{3\times6}$ of Eq. (36), which is simpler than the hybridization in SMM imposed on $\tilde{\boldsymbol{\kappa}}_k^u$ of Eq. (37) and $\tilde{\boldsymbol{\kappa}}_k^\sigma$ of Eq. (38). This attributes to the conceptual simplicity of TMM and GMM.

It is worth noting that some numerical methods such as SAFE and SCM are intrinsically immune to the incompatibility issue of metallic-composite laminates [18,33]. This is because most numerical methods do not exploit partial waves, and usually end up with solving an eigenvalue problem which can be easily realized by calling existing programming subroutines such as the MATLAB function *eig*. In this

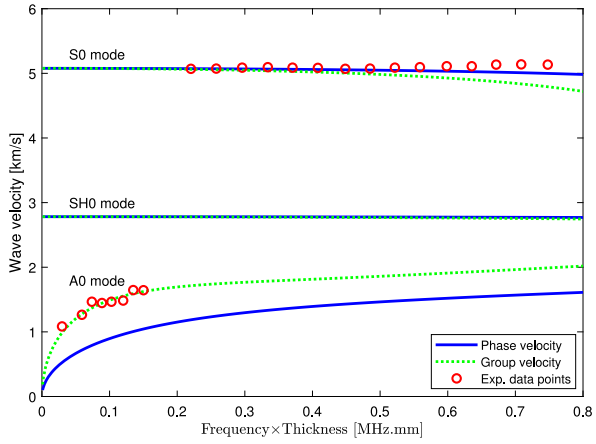

(a) $\theta = 0°$, the pure case

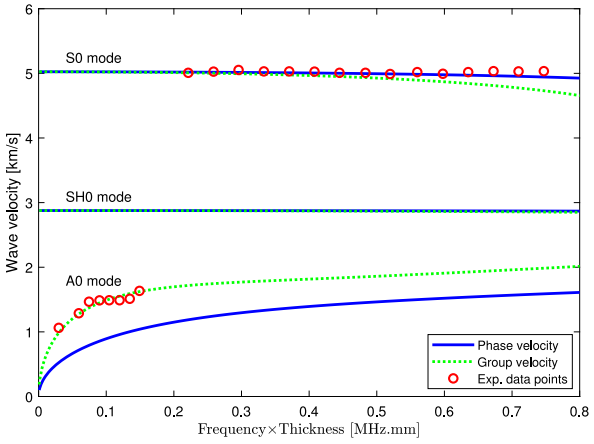

(b) $\theta = 20°$, the hybrid case

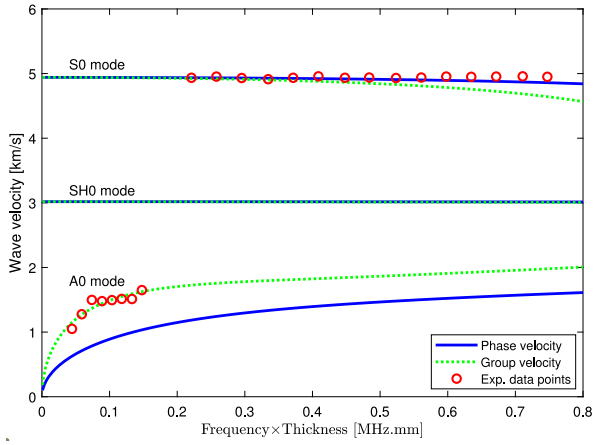

(c) $\theta = 45°$, the hybrid case

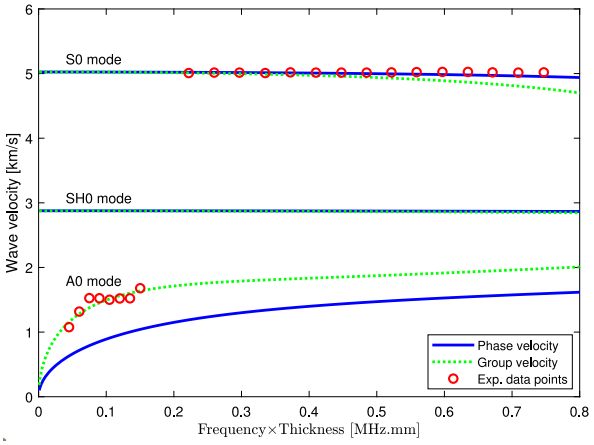

(d) $\theta = 70°$, the hybrid case

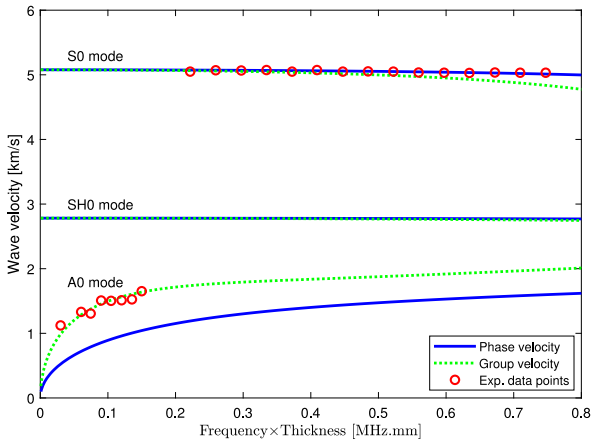

(e) $\theta = 90°$, the pure case

Fig. 11. Dispersion curves of the hybrid or pure Lamb and SH waves of the metallic-composite laminate. The experimental data points are extracted from [17].

regard, numerical methods is superior to the matrix-based methods. Nevertheless, one cannot wipe out the contribution of HMS to the state of the art solely based on this factor. Being theoretical approaches, GMM and SMM acted as the benchmark to evaluate the performance of various numerical methods [9,10]. Furthermore, HMS meticulously treats the interaction of guided waves with the metal–matrix interface, which is promising for studying the delamination issues of fiber-metal laminates [61]. Indeed, the occurrence of delamination at the metal–matrix interface usually gives rise to the reduction of interlaminar stiffness. Integrating HMS into delamination detection methods [62–64] to enhance their performance is an appealing perspective and will be comprehensively studied in the future.

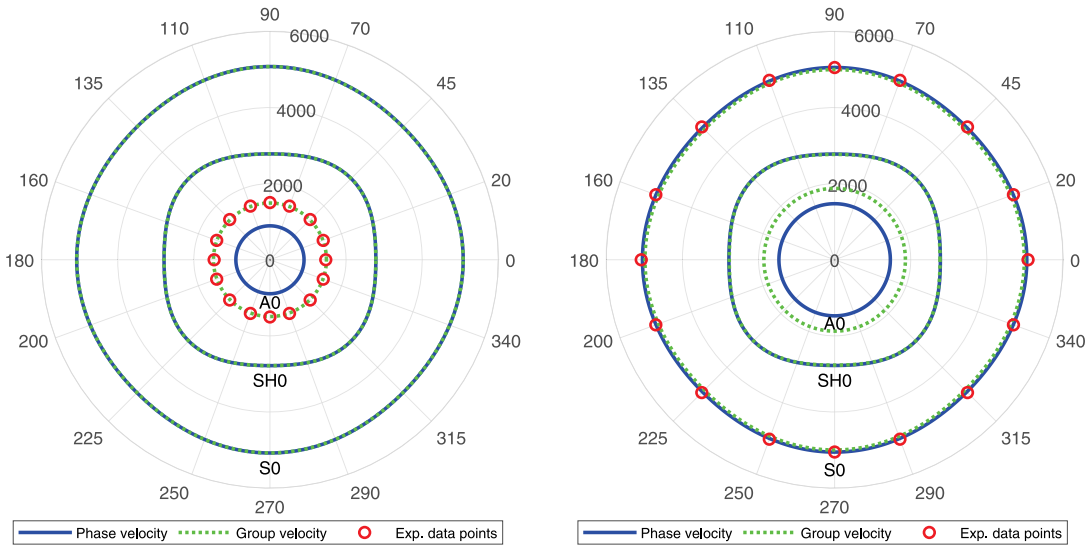

(a) $fd = 0.1\,\mathrm{MHz}\cdot\mathrm{mm}$ (b) $fd = 0.5\,\mathrm{MHz}\cdot\mathrm{mm}$

Fig. 12. Polar plot of wave velocity (unit: m/s). Four non-singular angles $\theta \in \{0°, 90°, 180°, 270°\}$ present in the metallic-composite laminate. The experimental data points are extracted from [17].

7. Conclusion

This paper comprehensively studies the coupling issue of guided waves propagation in arbitrarily stacked multi-layered composite plates. In accordance with different material classes in each layer of the laminate, there exists three cases of guided waves, namely, the coupled Lamb and SH waves, the separated Lamb and SH waves, and the hybrid case that in some layers of the laminate the two wave types are coupled to each other but in other layers decoupled. The hybrid case is generally existing in a quasi-isotropic composite plate and a metallic-composite plate for which metallic layers are isotropic but composite laminae are anisotropic.

The standard SMM can deal with the coupled and decoupled cases, but for the hybrid case, an original HMS is proposed to address the lamina stiffness matrix incompatibility issue. Its core idea is to hybridize the partial waves matrices of the pure Lamb and SH waves such that it is compatible with the counterpart of the coupled ones, thus guaranteeing the successful proceeding of the recursion process of generating the terminative stiffness matrix of the whole laminate system. The stability of HMS is interpreted in theory.

Numerical examples on two commonly used composite laminates, i.e. a quasi-isotropic laminate and a metallic-composite laminate, validates the effectiveness of the SMM-HMS framework, whose accuracy is further validated by the experimental data extracted from a classical Ref. [17]. The HMS is also superior to the pseudo correction measure for dealing with the incompatibility issue of metallic-composite plate.

The coupling case of guided waves in an arbitrarily stacked multi-layered composite plate may become irregular. Using the conceptual diagram to manually identify the singular angle is intuitional but cumbersome. The developed Algorithms 1–5, however, can automatically process the most inhomogeneous composite plates that are made up of the simplest isotropic, commonly used orthotropic and fully triclinic materials. Thus, the intelligence of SMM-HMS highlights its possibility of application in arbitrarily oriented multi-layered sandwich plate that is widely used in aeronautic and aerospace industry.

CRediT authorship contribution statement

Shuanglin Guo: Conceptualization, Methodology, Software, Investigation, Formal analysis, Writing – original draft. **Marc Rébillat:** Conceptualization, Methodology, Writing – original draft, Visualization, Supervision, Validation. **Yuan Liu:** Methodology, Software, Investigation, Formal analysis, Writing – original draft. **Qiufeng Li:** Validation, Writing – review & editing, Funding acquisition. **Chao Lu:** Validation, Writing – review & editing, Project administration, Funding acquisition. **Nazih Mechbal:** Conceptualization, Validation, Writing – review & editing, Supervision, Project administration.

Declaration of competing interest

The authors declared no potential conflicts of interest with respect to the research, authorship, and/or publication of this article.

Data availability

No data was used for the research described in the article.

Acknowledgments

We appreciate Dr. Shashank Pant for his approval of citing the experimental data in our paper and Prof. Eng Leong Tan who provided us his HCSMM papers which extend our understanding on the knowledge of SMM.

Funding

This work is supported by Key R&D plan of Jiangxi Province, China (Grant No. 20212BBE51006), Natural Science Foundation of Jiangxi Province, China (Grant No. 20212ACB204014, 20224BAB214052).

Appendix A. The polynomial coefficients in Eq. (10)

$$A_6 = -C_{35}^2 C_{44} + 2C_{34}C_{35}C_{45} - C_{33}C_{45}^2 - C_{34}^2 C_{55} + C_{33}C_{44}C_{55} \tag{A.1}$$

$$\begin{aligned} A_5 =& 2(-C_{15}C_{34}^2 + C_{14}C_{34}C_{35} + C_{15}C_{33}C_{44} - C_{13}C_{35}C_{44} \\ & - C_{14}C_{33}C_{45} + C_{13}C_{34}C_{45} + C_{35}C_{36}C_{45} - C_{35}^2 C_{46} \\ & - C_{34}C_{36}C_{55} + C_{33}C_{46}C_{55} + C_{34}C_{35}C_{56} - C_{33}C_{45}C_{56}) \end{aligned} \tag{A.2}$$

We firstly derive the hybrid lamina matrix of displacement $\widetilde{\boldsymbol{\kappa}}_k^u$.

The displacement field in Eq. (33) is expanded as follows with suppressing the phase term $\mathrm{e}^{\mathrm{i}\xi(x_1-vt)}$.

$$u_1 = U_1\mathrm{e}^{\mathrm{i}\xi\alpha_1 x_3}\eta_1 + U_1\mathrm{e}^{-\mathrm{i}\xi\alpha_1 x_3}\eta_2 + U_3\mathrm{e}^{\mathrm{i}\xi\alpha_3 x_3}\eta_3 + U_3\mathrm{e}^{-\mathrm{i}\xi\alpha_3 x_3}\eta_4 + 0\mathrm{e}^{\mathrm{i}\xi\alpha_5 x_3}\eta_5 + 0\mathrm{e}^{-\mathrm{i}\xi\alpha_5 x_3}\eta_6 \tag{C.1}$$

$$u_2 = 0\mathrm{e}^{\mathrm{i}\xi\alpha_1 x_3}\eta_1 + 0\mathrm{e}^{-\mathrm{i}\xi\alpha_1 x_3}\eta_2 + 0\mathrm{e}^{\mathrm{i}\xi\alpha_3 x_3}\eta_3 + 0\mathrm{e}^{-\mathrm{i}\xi\alpha_3 x_3}\eta_4 + V_5\mathrm{e}^{\mathrm{i}\xi\alpha_5 x_3}\eta_5 + V_5\mathrm{e}^{-\mathrm{i}\xi\alpha_5 x_3}\eta_6 \tag{C.2}$$

$$u_3 = W_1\mathrm{e}^{\mathrm{i}\xi\alpha_1 x_3}\eta_1 - W_1\mathrm{e}^{-\mathrm{i}\xi\alpha_1 x_3}\eta_2 + W_3\mathrm{e}^{\mathrm{i}\xi\alpha_3 x_3}\eta_3 - W_3\mathrm{e}^{-\mathrm{i}\xi\alpha_3 x_3}\eta_4 + 0\mathrm{e}^{\mathrm{i}\xi\alpha_5 x_3}\eta_5 + 0\mathrm{e}^{-\mathrm{i}\xi\alpha_5 x_3}\eta_6 \tag{C.3}$$

On the top side of layer l_k, its local coordinate $x_3^k = 0$, Eqs. (C.1)-(C.3) become Eqs. (C.4)-(C.6).

$$u_1^{\mathrm{T}} = U_1\eta_1 + U_1\eta_2 + U_3\eta_3 + U_3\eta_4 + 0\eta_5 + 0\eta_6 \tag{C.4}$$

$$u_2^{\mathrm{T}} = 0\eta_1 + 0\eta_2 + 0\eta_3 + 0\eta_4 + V_5\eta_5 + V_5\eta_6 \tag{C.5}$$

$$u_3^{\mathrm{T}} = W_1\eta_1 - W_1\eta_2 + W_3\eta_3 - W_3\eta_4 + 0\eta_5 + 0\eta_6 \tag{C.6}$$

On the bottom side of layer l_k, the local coordinate $x_3^k = d_k$, Eqs. (C.1)-(C.3) change to Eqs. (C.7)-(C.9).

$$u_1^{\mathrm{B}} = U_1\mathrm{e}^{\mathrm{i}\xi\alpha_1 d_k}\eta_1 + U_1\mathrm{e}^{-\mathrm{i}\xi\alpha_1 d_k}\eta_2 + U_3\mathrm{e}^{\mathrm{i}\xi\alpha_3 d_k}\eta_3 + U_3\mathrm{e}^{-\mathrm{i}\xi\alpha_3 d_k}\eta_4 + 0\mathrm{e}^{\mathrm{i}\xi\alpha_5 d_k}\eta_5 + 0\mathrm{e}^{-\mathrm{i}\xi\alpha_5 d_k}\eta_6 \tag{C.7}$$

$$u_2^{\mathrm{B}} = 0\mathrm{e}^{\mathrm{i}\xi\alpha_1 d_k}\eta_1 + 0\mathrm{e}^{-\mathrm{i}\xi\alpha_1 d_k}\eta_2 + 0\mathrm{e}^{\mathrm{i}\xi\alpha_3 d_k}\eta_3 + 0\mathrm{e}^{-\mathrm{i}\xi\alpha_3 d_k}\eta_4 + V_5\mathrm{e}^{\mathrm{i}\xi\alpha_5 d_k}\eta_5 + V_5\mathrm{e}^{-\mathrm{i}\xi\alpha_5 d_k}\eta_6 \tag{C.8}$$

$$u_3^{\mathrm{B}} = W_1\mathrm{e}^{\mathrm{i}\xi\alpha_1 d_k}\eta_1 - W_1\mathrm{e}^{-\mathrm{i}\xi\alpha_1 d_k}\eta_2 + W_3\mathrm{e}^{\mathrm{i}\xi\alpha_3 d_k}\eta_3 - W_3\mathrm{e}^{-\mathrm{i}\xi\alpha_3 d_k}\eta_4 + 0\mathrm{e}^{\mathrm{i}\xi\alpha_5 d_k}\eta_5 + 0\mathrm{e}^{-\mathrm{i}\xi\alpha_5 d_k}\eta_6 \tag{C.9}$$

Eqs. (C.4)-(C.6) can be equivalently written as Eqs. (C.10)-(C.12),
meanwhile Eqs. (C.7)-(C.9) are equivalently written as Eqs. (C.13)- (C.15).

$$u_1^{\mathrm{T}} = U_1\eta_1 + U_3\eta_3 + 0\eta_5 + U_1\mathrm{e}^{\mathrm{i}\xi\alpha_1 d_k}\mathrm{e}^{-\mathrm{i}\xi\alpha_1 d_k}\eta_2 + U_3\mathrm{e}^{\mathrm{i}\xi\alpha_3 d_k}\mathrm{e}^{-\mathrm{i}\xi\alpha_3 d_k}\eta_4 + 0\mathrm{e}^{\mathrm{i}\xi\alpha_5 d_k}\mathrm{e}^{-\mathrm{i}\xi\alpha_5 d_k}\eta_6 \tag{C.10}$$

$$u_2^{\mathrm{T}} = 0\eta_1 + 0\eta_3 + V_5\eta_5 + 0\mathrm{e}^{\mathrm{i}\xi\alpha_1 d_k}\mathrm{e}^{-\mathrm{i}\xi\alpha_1 d_k}\eta_2 + 0\mathrm{e}^{\mathrm{i}\xi\alpha_3 d_k}\mathrm{e}^{-\mathrm{i}\xi\alpha_3 d_k}\eta_4 + V_5\mathrm{e}^{\mathrm{i}\xi\alpha_5 d_k}\mathrm{e}^{-\mathrm{i}\xi\alpha_5 d_k}\eta_6 \tag{C.11}$$

$$u_3^{\mathrm{T}} = W_1\eta_1 + W_3\eta_3 + 0\eta_5 - W_1\mathrm{e}^{\mathrm{i}\xi\alpha_1 d_k}\mathrm{e}^{-\mathrm{i}\xi\alpha_1 d_k}\eta_2 - W_3\mathrm{e}^{\mathrm{i}\xi\alpha_3 d_k}\mathrm{e}^{-\mathrm{i}\xi\alpha_3 d_k}\eta_4 + 0\mathrm{e}^{\mathrm{i}\xi\alpha_5 d_k}\mathrm{e}^{-\mathrm{i}\xi\alpha_5 d_k}\eta_6 \tag{C.12}$$

$$u_1^{\mathrm{B}} = U_1\mathrm{e}^{\mathrm{i}\xi\alpha_1 d_k}\eta_1 + U_3\mathrm{e}^{\mathrm{i}\xi\alpha_3 d_k}\eta_3 + 0\mathrm{e}^{\mathrm{i}\xi\alpha_5 d_k}\eta_5 + U_1\mathrm{e}^{-\mathrm{i}\xi\alpha_1 d_k}\eta_2 + U_3\mathrm{e}^{-\mathrm{i}\xi\alpha_3 d_k}\eta_4 + 0\mathrm{e}^{-\mathrm{i}\xi\alpha_5 d_k}\eta_6 \tag{C.13}$$

$$u_2^{\mathrm{B}} = 0\mathrm{e}^{\mathrm{i}\xi\alpha_1 d_k}\eta_1 + 0\mathrm{e}^{\mathrm{i}\xi\alpha_3 d_k}\eta_3 + V_5\mathrm{e}^{\mathrm{i}\xi\alpha_5 d_k}\eta_5 + 0\mathrm{e}^{-\mathrm{i}\xi\alpha_1 d_k}\eta_2 + 0\mathrm{e}^{-\mathrm{i}\xi\alpha_3 d_k}\eta_4 + V_5\mathrm{e}^{-\mathrm{i}\xi\alpha_5 d_k}\eta_6 \tag{C.14}$$

$$u_3^{\mathrm{B}} = W_1\mathrm{e}^{\mathrm{i}\xi\alpha_1 d_k}\eta_1 + W_3\mathrm{e}^{\mathrm{i}\xi\alpha_3 d_k}\eta_3 + 0\mathrm{e}^{\mathrm{i}\xi\alpha_5 d_k}\eta_5 - W_1\mathrm{e}^{-\mathrm{i}\xi\alpha_1 d_k}\eta_2 - W_3\mathrm{e}^{-\mathrm{i}\xi\alpha_3 d_k}\eta_4 + 0\mathrm{e}^{-\mathrm{i}\xi\alpha_5 d_k}\eta_6 \tag{C.15}$$

Rewrite Eqs. (C.10)-(C.15) as the matrix form in Eq. (C.16), in which the matrix $\widetilde{\boldsymbol{\kappa}}_k^u$ is just defined as the hybrid lamina matrix of displacement in Eq. (37).

$$\begin{bmatrix} u_1^{\mathrm{T}} \\ u_2^{\mathrm{T}} \\ u_3^{\mathrm{T}} \\ u_1^{\mathrm{B}} \\ u_2^{\mathrm{B}} \\ u_3^{\mathrm{B}} \end{bmatrix} = \underbrace{\begin{bmatrix} U_1 & U_3 & 0 & U_1\mathrm{e}^{\mathrm{i}\xi\alpha_1 d_k} & U_3\mathrm{e}^{\mathrm{i}\xi\alpha_3 d_k} & 0 \\ 0 & 0 & V_5 & 0 & 0 & V_5\mathrm{e}^{\mathrm{i}\xi\alpha_5 d_k} \\ W_1 & W_3 & 0 & -W_1\mathrm{e}^{\mathrm{i}\xi\alpha_1 d_k} & -W_3\mathrm{e}^{\mathrm{i}\xi\alpha_3 d_k} & 0 \\ U_1\mathrm{e}^{\mathrm{i}\xi\alpha_1 d_k} & U_3\mathrm{e}^{\mathrm{i}\xi\alpha_3 d_k} & 0 & U_1 & U_3 & 0 \\ 0 & 0 & V_5\mathrm{e}^{\mathrm{i}\xi\alpha_5 d_k} & 0 & 0 & V_5 \\ W_1\mathrm{e}^{\mathrm{i}\xi\alpha_1 d_k} & W_3\mathrm{e}^{\mathrm{i}\xi\alpha_3 d_k} & 0 & -W_1 & -W_3 & 0 \end{bmatrix}}_{\widetilde{\boldsymbol{\kappa}}_k^u} \begin{bmatrix} \eta_1 \\ \eta_3 \\ \eta_5 \\ \mathrm{e}^{-\mathrm{i}\xi\alpha_1 d_k}\eta_2 \\ \mathrm{e}^{-\mathrm{i}\xi\alpha_3 d_k}\eta_4 \\ \mathrm{e}^{-\mathrm{i}\xi\alpha_5 d_k}\eta_6 \end{bmatrix} \tag{C.16}$$

With the similar derivation for the stress field in Eq. (35), the hybrid lamina matrix of stress $\widetilde{\boldsymbol{\kappa}}_k^\sigma$ in Eq. (38) can be deduced as the form in Eq. (C.17).

$$\begin{bmatrix} \sigma_{33}^{\mathrm{T}} \\ \sigma_{23}^{\mathrm{T}} \\ \sigma_{13}^{\mathrm{T}} \\ \sigma_{33}^{\mathrm{B}} \\ \sigma_{23}^{\mathrm{B}} \\ \sigma_{13}^{\mathrm{B}} \end{bmatrix} = \underbrace{\begin{bmatrix} \beta_{11} & \beta_{13} & 0 & \beta_{11}\mathrm{e}^{\mathrm{i}\xi\alpha_1 d_k} & \beta_{13}\mathrm{e}^{\mathrm{i}\xi\alpha_3 d_k} & 0 \\ 0 & 0 & \beta_{25} & 0 & 0 & -\beta_{25}\mathrm{e}^{\mathrm{i}\xi\alpha_5 d_k} \\ \beta_{31} & \beta_{33} & 0 & -\beta_{31}\mathrm{e}^{\mathrm{i}\xi\alpha_1 d_k} & -\beta_{33}\mathrm{e}^{\mathrm{i}\xi\alpha_3 d_k} & 0 \\ \beta_{11}\mathrm{e}^{\mathrm{i}\xi\alpha_1 d_k} & \beta_{13}\mathrm{e}^{\mathrm{i}\xi\alpha_3 d_k} & 0 & \beta_{11} & \beta_{13} & 0 \\ 0 & 0 & \beta_{25}\mathrm{e}^{\mathrm{i}\xi\alpha_5 d_k} & 0 & 0 & -\beta_{25} \\ \beta_{31}\mathrm{e}^{\mathrm{i}\xi\alpha_1 d_k} & \beta_{33}\mathrm{e}^{\mathrm{i}\xi\alpha_3 d_k} & 0 & -\beta_{31} & -\beta_{33} & 0 \end{bmatrix}}_{\widetilde{\boldsymbol{\kappa}}_k^\sigma} \begin{bmatrix} \eta_1 \\ \eta_3 \\ \eta_5 \\ \mathrm{e}^{-\mathrm{i}\xi\alpha_1 d_k}\eta_2 \\ \mathrm{e}^{-\mathrm{i}\xi\alpha_3 d_k}\eta_4 \\ \mathrm{e}^{-\mathrm{i}\xi\alpha_5 d_k}\eta_6 \end{bmatrix} \tag{C.17}$$

Fig. C.13. Derivation of the hybrid lamina matrices of displacement and stress.

$$\begin{aligned} A_4 = &- C_{14}^2C_{33} - C_{11}C_{34}^2 + 2C_{16}C_{34}C_{35} - 4C_{15}C_{34}C_{36} - C_{13}^2C_{44} \\ &+ C_{11}C_{33}C_{44} + 2C_{15}C_{35}C_{44} - 2C_{16}C_{33}C_{45} \\ &- 2C_{15}C_{34}C_{45} + 2C_{13}C_{36}C_{45} \\ &+ 2C_{13}C_{45}^2 + 4C_{15}C_{33}C_{46} - 4C_{13}C_{35}C_{46} - C_{36}^2C_{55} \\ &- 2C_{13}C_{44}C_{55} + 2C_{13}C_{34}C_{56} \\ &+ 2C_{35}C_{36}C_{56} - C_{33}C_{56}^2 + 2C_{14}(C_{13}C_{34} + C_{35}C_{36} \\ &- C_{35}C_{45} + C_{34}C_{55} - C_{33}C_{56}) \\ &- C_{35}^2C_{66} + C_{33}C_{55}C_{66} \\ &+ \left(C_{34}^2 + C_{35}^2 - C_{33}C_{44} + C_{45}^2 - C_{33}C_{55} - C_{44}C_{55}\right)\rho v^2 \end{aligned} \tag{A.3}$$

$$\begin{aligned} A_3 = &2[- C_{14}^2C_{35} - C_{11}C_{34}C_{36} + C_{16}C_{35}C_{36} - C_{15}C_{36}^2 + C_{11}C_{35}C_{44} \\ &- C_{11}C_{34}C_{45} - C_{16}C_{35}C_{45} - C_{15}C_{36}C_{45} - C_{13}^2C_{46} + C_{11}C_{33}C_{46} \\ &+ 2C_{34}C_{35}C_{46} + C_{16}C_{34}C_{55} - C_{16}C_{33}C_{56} - C_{15}C_{34}C_{56} \\ &+ C_{14}(-C_{16}C_{33} + C_{15}C_{34} + C_{13}C_{36} + C_{13}C_{45} + C_{36}C_{55} - C_{35}C_{56}) \\ &+ C_{15}C_{33}C_{66} + C_{13}(C_{16}C_{34} - C_{15}C_{44} - 2C_{46}C_{55} \\ &+ C_{36}C_{56} + 2C_{45}C_{56} - C_{35}C_{66})] \\ &+ 2[C_{13}C_{35} + C_{34}C_{36} - C_{35}C_{44} - C_{15}(C_{33} + C_{44}) + C_{14}C_{45} \\ &+ C_{34}C_{45} - C_{33}C_{46} - C_{46}C_{55} + C_{45}C_{56}]\rho v^2 \end{aligned} \tag{A.4}$$

$$
\begin{aligned}
A_2 =& -C_{16}^2C_{33} - C_{11}C_{36}^2 - C_{15}^2C_{44} - 2C_{11}C_{36}C_{45} - C_{11}C_{45}^2 - 4C_{13}C_{15}C_{46} \\
&+ 4C_{11}C_{35}C_{46} - C_{14}^2C_{55} + C_{11}C_{44}C_{55} - 2C_{11}C_{34}C_{56} \\
&- 2C_{15}C_{36}C_{56} + 2C_{13}C_{56}^2 \\
&+ 2C_{14}[C_{15}(C_{36} + C_{45}) + C_{13}C_{56}] \\
&+ 2C_{16}(C_{15}C_{34} - 2C_{14}C_{35} + C_{13}C_{36} + C_{13}C_{45} \\
&+ C_{36}C_{55} - C_{35}C_{56}) - C_{13}^2C_{66} \\
&+ C_{11}C_{33}C_{66} + 2C_{15}C_{35}C_{66} - 2C_{13}C_{55}C_{66} \\
&+ (C_{13}^2 + C_{14}^2 - C_{11}C_{33} - 2C_{15}C_{35} + C_{36}^2 - C_{11}C_{44} \\
&+ 2C_{16}C_{45} + 2C_{36}C_{45} + C_{45}^2 \\
&- 4C_{15}C_{46} - 4C_{35}C_{46} + 2C_{13}C_{55} - C_{44}C_{55} + 2C_{14}C_{56} \\
&+ 2C_{34}C_{56} + C_{56}^2 - C_{33}C_{66} \\
&- C_{55}C_{66})\rho v^2 + (C_{33} + C_{44} + C_{55})\left(\rho v^2\right)^2
\end{aligned}
\tag{A.5}
$$

$$
\begin{aligned}
A_1 =& 2(-C_{16}^2C_{35} - C_{15}^2C_{46} + C_{16}(C_{15}(C_{36} + C_{45}) \\
&- C_{14}C_{55} + C_{13}C_{56}) + C_{15}(C_{14}C_{56} - C_{13}C_{66}) \\
&+ C_{11}(C_{46}C_{55} - C_{36}C_{56} - C_{45}C_{56} + C_{35}C_{66})) \\
&+ 2(C_{13}C_{15} + C_{14}C_{16} - C_{11}C_{35} - C_{11}C_{46} \\
&- C_{46}C_{55} + C_{16}C_{56} + C_{36}C_{56} + C_{45}C_{56} - C_{15}C_{66} - C_{35}C_{66})\rho v^2 \\
&+ 2(C_{15} + C_{35} + C_{46})\left(\rho v^2\right)^2
\end{aligned}
\tag{A.6}
$$

$$
\begin{aligned}
A_0 =& -C_{16}^2C_{55} + 2C_{15}C_{16}C_{56} - C_{11}C_{56}^2 - C_{15}^2C_{66} + C_{11}C_{55}C_{66} \\
&+ (C_{15}^2 + C_{16}^2 - C_{11}C_{55} + C_{56}^2 - C_{11}C_{66} - C_{55}C_{66})\rho v^2 \\
&+ \left(C_{11} + C_{55} + C_{66}\right)\left(\rho v^2\right)^2 - \left(\rho v^2\right)^3
\end{aligned}
\tag{A.7}
$$

Appendix B. Proof of Eq. (28)

The core idea of proving Eq. (28) is to apply the displacement and stress continuity condition formulized in Eqs. (B.1a) and (B.1b). See the interface i_{k-1} in Fig. 4(b) for easy understanding.

$$\mathbf{u}_{k-1}^{\mathrm{B}} = \mathbf{u}_k^{\mathrm{T}} \tag{B.1a}$$

$$\boldsymbol{\sigma}_{k-1}^{\mathrm{B}} = \boldsymbol{\sigma}_k^{\mathrm{T}} \tag{B.1b}$$

Expanding Eq. (29) into Eqs. (B.2a) and (B.2b).

$$\boldsymbol{\sigma}_1^{\mathrm{T}} = \mathbf{K}_{k-1}^{\mathrm{TT}}\mathbf{u}_1^{\mathrm{T}} + \mathbf{K}_{k-1}^{\mathrm{TB}}\mathbf{u}_{k-1}^{\mathrm{B}} \tag{B.2a}$$

$$\boldsymbol{\sigma}_{k-1}^{\mathrm{B}} = \mathbf{K}_{k-1}^{\mathrm{BT}}\mathbf{u}_1^{\mathrm{T}} + \mathbf{K}_{k-1}^{\mathrm{BB}}\mathbf{u}_{k-1}^{\mathrm{B}} \tag{B.2b}$$

Due to the continuity condition in Eqs. (B.1a) and (B.1b), $\mathbf{u}_{k-1}^{\mathrm{B}}$ and $\boldsymbol{\sigma}_{k-1}^{\mathrm{B}}$ in Eqs. (B.2a) and (B.2b) can be replaced by $\mathbf{u}_k^{\mathrm{T}}$ and $\boldsymbol{\sigma}_k^{\mathrm{T}}$, respectively, thus Eqs. (B.3a) and (B.3b) are obtained.

$$\boldsymbol{\sigma}_1^{\mathrm{T}} = \mathbf{K}_{k-1}^{\mathrm{TT}}\mathbf{u}_1^{\mathrm{T}} + \mathbf{K}_{k-1}^{\mathrm{TB}}\mathbf{u}_k^{\mathrm{T}} \tag{B.3a}$$

$$\boldsymbol{\sigma}_k^{\mathrm{T}} = \mathbf{K}_{k-1}^{\mathrm{BT}}\mathbf{u}_1^{\mathrm{T}} + \mathbf{K}_{k-1}^{\mathrm{BB}}\mathbf{u}_k^{\mathrm{T}} \tag{B.3b}$$

With the block matrices in Eq. (26), Eq. (25) is expanded into Eqs. (B.4a) and (B.4b).

$$\boldsymbol{\sigma}_k^{\mathrm{T}} = \boldsymbol{\kappa}_k^{\mathrm{TT}}\mathbf{u}_k^{\mathrm{T}} + \boldsymbol{\kappa}_k^{\mathrm{TB}}\mathbf{u}_k^{\mathrm{B}} \tag{B.4a}$$

$$\boldsymbol{\sigma}_k^{\mathrm{B}} = \boldsymbol{\kappa}_k^{\mathrm{BT}}\mathbf{u}_k^{\mathrm{T}} + \boldsymbol{\kappa}_k^{\mathrm{BB}}\mathbf{u}_k^{\mathrm{B}} \tag{B.4b}$$

Eqs. (B.3b) and (B.4a) represent the same variable $\boldsymbol{\sigma}_k^{\mathrm{T}}$, which makes Eq. (B.5).

$$\mathbf{K}_{k-1}^{\mathrm{BT}}\mathbf{u}_1^{\mathrm{T}} + \mathbf{K}_{k-1}^{\mathrm{BB}}\mathbf{u}_k^{\mathrm{T}} = \boldsymbol{\kappa}_k^{\mathrm{TT}}\mathbf{u}_k^{\mathrm{T}} + \boldsymbol{\kappa}_k^{\mathrm{TB}}\mathbf{u}_k^{\mathrm{B}} \tag{B.5}$$

$\mathbf{u}_k^{\mathrm{T}}$ is solved into Eq. (B.6) from Eq. (B.5).

$$\mathbf{u}_k^{\mathrm{T}} = \left(\boldsymbol{\kappa}_k^{\mathrm{TT}} - \mathbf{K}_{k-1}^{\mathrm{BB}}\right)^{-1}\mathbf{K}_{k-1}^{\mathrm{BT}}\mathbf{u}_1^{\mathrm{T}} - \left(\boldsymbol{\kappa}_k^{\mathrm{TT}} - \mathbf{K}_{k-1}^{\mathrm{BB}}\right)^{-1}\boldsymbol{\kappa}_k^{\mathrm{TB}}\mathbf{u}_k^{\mathrm{B}} \tag{B.6}$$

Substituting Eq. (B.6) into Eq. (B.3a) leads to Eq. (B.7).

$$\boldsymbol{\sigma}_1^{\mathrm{T}} = \left[\mathbf{K}_{k-1}^{\mathrm{TT}} + \mathbf{K}_{k-1}^{\mathrm{TB}}\left(\boldsymbol{\kappa}_k^{\mathrm{TT}} - \mathbf{K}_{k-1}^{\mathrm{BB}}\right)^{-1}\mathbf{K}_{k-1}^{\mathrm{BT}}\right]\mathbf{u}_1^{\mathrm{T}} - \mathbf{K}_{k-1}^{\mathrm{TB}}\left(\boldsymbol{\kappa}_k^{\mathrm{TT}} - \mathbf{K}_{k-1}^{\mathrm{BB}}\right)^{-1}\boldsymbol{\kappa}_k^{\mathrm{TB}}\mathbf{u}_k^{\mathrm{B}} \tag{B.7}$$

Substituting Eq. (B.6) into Eq. (B.4b) leads to Eq. (B.8).

$$\boldsymbol{\sigma}_k^{\mathrm{B}} = \boldsymbol{\kappa}_k^{\mathrm{BT}}\left(\boldsymbol{\kappa}_k^{\mathrm{TT}} - \mathbf{K}_{k-1}^{\mathrm{BB}}\right)^{-1}\mathbf{K}_{k-1}^{\mathrm{BT}}\mathbf{u}_1^{\mathrm{T}} + \left[\boldsymbol{\kappa}_k^{\mathrm{BB}} - \boldsymbol{\kappa}_k^{\mathrm{BT}}\left(\boldsymbol{\kappa}_k^{\mathrm{TT}} - \mathbf{K}_{k-1}^{\mathrm{BB}}\right)^{-1}\boldsymbol{\kappa}_k^{\mathrm{TB}}\right]\mathbf{u}_k^{\mathrm{B}} \tag{B.8}$$

Rearranging Eqs. (B.7) and (B.8) as matrix form just proves Eq. (28).

Appendix C. Proof of Eqs. (37) and (38)

The derivation of $\tilde{\boldsymbol{\kappa}}_k^u$ and $\tilde{\boldsymbol{\kappa}}_k^\sigma$ in Eqs. (37) and (38) is illustrated in Fig. C.13. The procedures stated in this figure are also applicable for proving $\boldsymbol{\kappa}_k^u$ and $\boldsymbol{\kappa}_k^\sigma$ in Fig. 5 and Eqs. (45) and (46).

References

[1] Giurgiutiu Victor. Structural health monitoring of aerospace composites. Academic Press; 2015.
[2] Su Zhongqing, Ye Lin. Identification of damage using lamb waves: from fundamentals to applications. Vol. 48. Springer Science & Business Media; 2009.
[3] Lammering Rolf, Gabbert Ulrich, Sinapius Michael, Schuster Thomas, Wierach Peter. Lamb-wave based structural health monitoring in polymer composites. Springer; 2017.
[4] Mitra Mira, Gopalakrishnan S. Guided wave based structural health monitoring: A review. Smart Mater Struct 2016;25(5):053001.
[5] Lamb Horace. On waves in an elastic plate. Proc R Soc Lond Ser A Contain Pap Math. Phys Char 1917;93(648):114–28.
[6] Auld Bertram Alexander. Acoustic fields and waves in solids. John Wiley and Sons; 1973.
[7] Wilcox P, Lowe M, Cawley P. The effect of dispersion on long-range inspection using ultrasonic guided waves. NDT E Int 2001;34(1):1–9.
[8] Wilcox PD, Lowe MJS, Cawley P. Mode and transducer selection for long range lamb wave inspection. J Intell Mater Syst Struct 2001;12(8):553–65.
[9] Barazanchy Darun, Giurgiutiu Victor. A comparative convergence and accuracy study of composite guided-ultrasonic wave solution methods: Comparing the unified analytic method, SAFE method and DISPERSE. Proc Inst Mech Eng C 2017;231(16):2961–73.
[10] Orta Adil Han, Kersemans Mathias, Van Den Abeele Koen. A comparative study for calculating dispersion curves in viscoelastic multi-layered plates. Compos Struct 2022;115779.
[11] Haskell Norman A. The dispersion of surface waves on multilayered media. Bull Seismol Soc Am 1953;43(1):17–34.
[12] Nayfeh Adnan H. Wave propagation in layered anisotropic media: with applications to composites. Elsevier; 1995.
[13] Knopoff L. A matrix method for elastic wave problems. Bull Seismol Soc Am 1964;54(1):431–8.
[14] Lowe Michael JS. Matrix techniques for modeling ultrasonic waves in multilayered media. IEEE Trans Ultrason Ferroelectr Freq Control 1995;42(4):525–42.
[15] Wang Luck, Rokhlin SI. Stable reformulation of transfer matrix method for wave propagation in layered anisotropic media. Ultrasonics 2001;39(6):413–24.
[16] Rokhlin SI, Wang L. Stable recursive algorithm for elastic wave propagation in layered anisotropic media: Stiffness matrix method. J Acoust Soc Am 2002;112(3):822–34.
[17] Pant S, Laliberte Jeremy, Martinez Marcias, Rocha B. Derivation and experimental validation of lamb wave equations for an n-layered anisotropic composite laminate. Compos Struct 2014;111:566–79.
[18] Quintanilla F Hernando, Lowe MJS, Craster RV. Modeling guided elastic waves in generally anisotropic media using a spectral collocation method. J Acoust Soc Am 2015;137(3):1180–94.
[19] Nandyala Anvesh R, Darpe Ashish K, Singh Satinder P. Effective stiffness matrix method for predicting the dispersion curves in general anisotropic composites. Arch Appl Mech 2019;89(9):1923–38.
[20] Neau G. Lamb waves in anisotropic viscoelastic plates. Study of the wave fronts and attenuation (Ph.D. thesis), L'Universite de Bordeaux; 2003.
[21] Maghsoodi Ameneh, Ohadi Abdolreza, Sadighi Mojtaba. Calculation of wave dispersion curves in multilayered composite-metal plates. Shock Vib 2014;2014.
[22] Guo Shuanglin. Contribution to the study of guided waves propagation and attenuation in anisotropic composite laminates made up of viscoelastic composite materials: Application to A380 mounted nacelle parts (Ph.D. thesis), ENSAM, Paris, France; 2021.

[23] Wang Lei, Yuan FG. Group velocity and characteristic wave curves of Lamb waves in composites: Modeling and experiments. Compos Sci Technol 2007;67(7–8):1370–84.
[24] Ramasawmy Danny R, Cox Ben T, Treeby Bradley E. ElasticMatrix: A MATLAB toolbox for anisotropic elastic wave propagation in layered media. SoftwareX 2020;11:100397.
[25] Lowe M, Pavlakovic B. DISPERSE: A system for generating dispersion curves, User's Manual version 2.0. 20a. Imperial College London; 2013.
[26] Kamal Ayman, Giurgiutiu Victor. Stiffness Transfer Matrix Method (STMM) for stable dispersion curves solution in anisotropic composites. In: Health monitoring of structural and biological systems 2014. Vol. 9064. SPIE; 2014, p. 293–306.
[27] Muc A, Barski M, Stawiarski A, Chwał M, Augustyn M. Dispersion curves and identification of elastic wave modes for fiber metal laminates. Compos Struct 2021;255:112930.
[28] Huber Armin MA, Sause Markus GR. Classification of solutions for guided waves in anisotropic composites with large numbers of layers. J Acoust Soc Am 2018;144(6):3236–51.
[29] Tan Eng Leong. Stiffness matrix method with improved efficiency for elastic wave propagation in layered anisotropic media. J Acoust Soc Am 2005;118(6):3400–3.
[30] Tan Eng Leong. Hybrid compliance-stiffness matrix method for stable analysis of elastic wave propagation in multilayered anisotropic media. J Acoust Soc Am 2006;119(1):45–53.
[31] Tan Eng Leong. Matrix algorithms for modeling acoustic waves in piezoelectric multilayers. IEEE Trans Ultrason Ferroelectr Freq Control 2007;54(10):2016–23.
[32] Tan Eng Leong. Recursive asymptotic hybrid matrix method for acoustic waves in multilayered piezoelectric media. Open J Acoust 2011;1(02):27.
[33] Bartoli Ivan, Marzani Alessandro, Di Scalea Francesco Lanza, Viola Erasmo. Modeling wave propagation in damped waveguides of arbitrary cross-section. J Sound Vib 2006;295(3–5):685–707.
[34] Bocchini Paolo, Marzani Alessandro, Viola Erasmo. Graphical user interface for guided acoustic waves. J Comput Civ Eng 2011;25(3):202–10.
[35] Mace Brian R, Manconi Elisabetta. Modelling wave propagation in two-dimensional structures using finite element analysis. J Sound Vib 2008;318(4–5):884–902.
[36] Sorohan Ştefan, Constantin Nicolae, Găvan Mircea, Anghel Viorel. Extraction of dispersion curves for waves propagating in free complex waveguides by standard finite element codes. Ultrasonics 2011;51(4):503–15.
[37] Adamou ATI, Craster RV. Spectral methods for modelling guided waves in elastic media. J Acoust Soc Am 2004;116(3):1524–35.
[38] Quintanilla F Hernando, Lowe MJS, Craster RV. Full 3D dispersion curve solutions for guided waves in generally anisotropic media. J Sound Vib 2016;363:545–59.
[39] Kiefer Daniel A, Ponschab Michael, Rupitsch Stefan J, Mayle Michael. Calculating the full leaky Lamb wave spectrum with exact fluid interaction. J Acoust Soc Am 2019;145(6):3341–50.
[40] Georgiades Evripides, Lowe Michael JS, Craster Richard V. Leaky wave characterisation using spectral methods. J Acoust Soc Am 2022;152(3):1487–97.
[41] Wang Lei, Yuan FG. Lamb wave propagation in composite laminates using a higher-order plate theory. In: Nondestructive characterization for composite materials, aerospace engineering, civil infrastructure, and homeland security 2007. Vol. 6531. International Society for Optics and Photonics; 2007, p. 65310I.
[42] Zhao Jinling, Ji Hongli, Qiu Jinhao. Modeling of Lamb waves in composites using new third-order plate theories. Smart Mater Struct 2014;23(4):045017.
[43] Orta Adil Han, Vandendriessche Jeroen, Kersemans Mathias, Van Paepegem Wim, Roozen Nicolaas Bernardus, Van Den Abeele Koen. Modeling lamb wave propagation in visco-elastic composite plates using a fifth-order plate theory. Ultrasonics 2021;116:106482.
[44] He Cunfu, Liu Hongye, Liu Zenghua, Wu Bin. The propagation of coupled lamb waves in multilayered arbitrary anisotropic composite laminates. J Sound Vib 2013;332(26):7243–56.
[45] Dahmen Souhail, Amor Morched Ben, Ghozlen Mohamed Hédi Ben. Investigation of the coupled lamb waves propagation in viscoelastic and anisotropic multilayer composites by Legendre polynomial method. Compos Struct 2016;153:557–68.
[46] Zhang Xiaoming, Li Zhi, Yu Jiangong. The Computation of complex dispersion and properties of evanescent Lamb wave in Functionally graded piezoelectric-piezomagnetic plates. Materials 2018;11(7):1186.
[47] Stoklasová Pavla, Sedlák Petr, Seiner Hanuš, Landa Michal. Forward and inverse problems for surface acoustic waves in anisotropic media: A Ritz–Rayleigh method based approach. Ultrasonics 2015;56:381–9.
[48] Grabec Tomáš, Sedlák Petr, Seiner Hanuš. Application of the Ritz–Rayleigh method for Lamb waves in extremely anisotropic media. Wave Motion 2020;96:102567.
[49] Tewary Vinod K. Green's-function method for modeling surface acoustic wave dispersion in anisotropic material systems and determination of material parameters. Wave Motion 2004;40(4):399–412.
[50] Karmazin Alexander, Kirillova Evgenia, Seemann Wolfgang, Syromyatnikov Pavel. Investigation of Lamb elastic waves in anisotropic multilayered composites applying the Green's matrix. Ultrasonics 2011;51(1):17–28.
[51] Nayfeh Adnan H. The general problem of elastic wave propagation in multilayered anisotropic media. J Acoust Soc Am 1991;89(4):1521–31.
[52] Rose Joseph L. Ultrasonic guided waves in solid media. Cambridge University Press; 2014.
[53] Barazanchy Darun, Giurgiutiu Victor. A unified formulation for predictive modeling of guided-ultrasonic wave dispersion curves in metallic and composite materials. J Intell Mater Syst Struct 2017;28(10):1272–86.
[54] Barski Marek, Pajak Piotr. Determination of dispersion curves for composite materials with the use of stiffness matrix method. Acta Mech Autom 2017;11(2).
[55] Gibson Ronald F. Principles of composite material mechanics. fourth ed. CRC Press; 2016.
[56] Press William H, Teukolsky Saul A, Vetterling William T, Flannery Brian P. Numerical recipes 3rd edition: the art of scientific computing. Cambridge University Press; 2007.
[57] Guo Shuanglin, Rébillat Marc, Mechbal Nazih. Dichotomy property of dispersion equation of guided waves propagating in anisotropic composite plates. Mech Syst Signal Process 2022;164:108212.
[58] Rokhlin Stanislav, Chimenti Dale, Nagy Peter. Physical ultrasonics of composites. Oxford University Press; 2011.
[59] Yang Zhengyan, Yang Lei, Zhang Jiaqi, Ma Shuyi, Tian Tong, Deng Deshuang, et al. Damage shape recognition algorithm of composite woven fabric plate based on guided waves. Compos Struct 2023;303:116351.
[60] Guo Shuanglin, Rébillat Marc, Mechbal Nazih. Prediction of frequency and spatially dependent attenuation of guided waves propagating in mounted and unmounted A380 parts made up of anisotropic viscoelastic composite laminates. Struct Health Monit 2022;14759217221099967.
[61] Chai Gin Boay, Manikandan Periyasamy. Low velocity impact response of fibre-metal laminates–A review. Compos Struct 2014;107:363–81.
[62] Mei Hanfei, Giurgiutiu Victor. Characterization of multilayer delaminations in composites using wavenumber analysis: numerical and experimental studies. Struct Health Monit 2021;20(3):1004–29.
[63] Ghrib Meriem, Berthe Laurent, Mechbal Nazih, Rébillat Marc, Guskov Mikhail, Ecault Romain, et al. Generation of controlled delaminations in composites using symmetrical laser shock configuration. Compos Struct 2017;171:286–97.
[64] Liu Yuan, Hong Xiaobin, Zhang Bin. Contact delamination detection of anisotropic composite plates using non-elliptical probability imaging of nonlinear ultrasonic guided waves. Struct Health Monit 2022;14759217221085159.